TALLINN UNIVERSITY OF TECHNOLOGY
SCHOOL OF ENGINEERING
Department of Materials and Environmental Technology

PHOTOLUMINESCENCE STUDY OF DEFECTS IN Sb_2Se_3

Sb_2Se_3 DEFEKTSTRUKTUURI UURINGUD KASUTADES FOTOLUMINESTSENTS SPEKTROSKOOPIAT

MASTER THESIS

Üliõpilane: İdil Mengü

Üliõpilaskood: 194362KAYM

Juhendaja: Prof. Maarja Grossberg

Tallinn 2021

(*On the reverse side of title page*)

AUTHOR'S DECLARATION

Hereby I declare, that I have written this thesis independently.
No academic degree has been applied for based on this material. All works, major viewpoints and data of the other authors used in this thesis have been referenced.

"....." ..... 20…..

Author: .....
/signature /

Thesis is in accordance with terms and requirements

"....." ..... 20….

Supervisor: ….....
/signature/

Accepted for defence

"....."..... 20… .

Chairman of theses defence commission: .....
/name and signature/

Non-exclusive licence for reproduction and publication of a graduation thesis[1]

I İdil Mengü

1. grant Tallinn University of Technology free licence (non-exclusive licence) for my thesis Study of defects in Sb_2Se_3 by photoluminescence spectroscopy,

supervised by Prof. Maarja Grossberg,

1.1 to be reproduced for the purposes of preservation and electronic publication of the graduation thesis, incl. to be entered in the digital collection of the library of Tallinn University of Technology until expiry of the term of copyright;

1.2 to be published via the web of Tallinn University of Technology, incl. to be entered in the digital collection of the library of Tallinn University of Technology until expiry of the term of copyright.

2. I am aware that the author also retains the rights specified in clause 1 of the non-exclusive licence.

3. I confirm that granting the non-exclusive licence does not infringe other persons' intellectual property rights, the rights arising from the Personal Data Protection Act or rights arising from other legislation.

21.05.2021

[1] *The non-exclusive licence is not valid during the validity of access restriction indicated in the student's application for restriction on access to the graduation thesis that has been signed by the school's dean, except in case of the university's right to reproduce the thesis for preservation purposes only. If a graduation thesis is based on the joint creative activity of two or more persons and the co-author(s) has/have not granted, by the set deadline, the student defending his/her graduation thesis consent to reproduce and publish the graduation thesis in compliance with clauses 1.1 and 1.2 of the non-exclusive licence, the non-exclusive license shall not be valid for the period.*

Department of Materials and Environmental Technology

THESIS TASK

Student: İdil Mengü, 194362KAYM

Study programme, Materials and Processes for Sustainable Energetics

main speciality: Processes for sustainable energetics

Supervisor(s): Prof. Maarja Grossberg, 620 3210

Thesis topic:

(in English) Study of defects in Sb_2Se_3 by photoluminescence spectroscopy

(in Estonian) Sb_2Se_3 defektstruktuuri uuringud kasutades fotoluminestsents spektroskoopiat

Thesis main objectives:

1. To familiarize with photoluminescence spectroscopy method
2. To learn the analysis process of photoluminescence measurement results by studying the emission of Sb_2Se_3 microcrystals
3. To gain knowledge about defects in Sb_2Se_3

Thesis tasks and time schedule:

No	Task description	Deadline
1.	Photoluminescence and Raman measurements of Sb_2Se_3 microcrystals. Writing literature review.	November 2020
2.	Analysis of the obtained experimental data.	March 2021
3.	Writing of a master's thesis.	May 2021

Language: English **Deadline for submission of thesis:** "21"May 2021

Student: İdil Mengü "....."…….....201….a

/signature/

Supervisor: Maarja Grossberg "....."....201….a

/signature/

Head of study programme: Sergei Bereznev "....."....201.a

/signature/

Terms of thesis closed defence and/or restricted access conditions to be formulated on the reverse side

Table of Contents

PREFACE

The topic of this master's thesis was initiated and the thesis work supervised by Prof. Maarja Grossberg, the Head of the Laboratory of Optoelectronic Materials Physics in the Department of Materials and Environmental Technology. Major part of the thesis work was carried out in the Laboratory of Optoelectronic Materials Physics. Senior researcher Dr. Kristi Timmo from the Laboratory of Photovoltaic Materials Research synthesized the studied Sb_2Se_3 microcrystals. PhD student Reelika Kaupmees assisted author in photoluminescence data collecting. Dr. Rokas Kondrotas from FTMC in Vilnius performed the XRD analysis and Dr. Valdek Mikli made the EDX analysis of the studied samples.

My special appreciation goes to my family members for their endless support, encouragement and love. Moreover, I would like to send my deepest gratitude to my supervisor Prof. Maarja Grossberg for giving me the opportunity to work on this project and to thank her for her guidance, patience and care. I would also like to thank my classmates for their companion and help to experience this period in the most positive way.

The study was financially supported by the Estonian Research Council grant PRG1023 "Sustainable, cost-efficient, flexible, lightweight and semitransparent multinary chalcogenide based solar cells for building integrated photovoltaics", by the European Regional Development Fund project TK141 "Advanced materials and high-technology devices for sustainable energetics, sensorics and nanoelectronics", and by the project "Center of nanomaterials technologies and research (NAMUR+)" (2014-2020.4.01.16-0123).

Keywords: Photoluminescence spectroscopy, defects, Sb_2Se_3, Raman spectroscopy, Master's thesis.

List of abbreviations and symbols

a-Sb_2Se_3	Amorphous antimony selenide
AS	Admittance spectroscopy
c-Sb_2Se_3	Crystalline antimony selenide
CBM	Conduction band minimum
CdS	Cadmium sulfide
CdTe	Cadmium telluride
CIGS	Copper indium gallium diselenide
CIS	Copper indium diselenide
CSS	Close-spaced sublimation
DAP	Donor-acceptor pair
DLTS	Deep level transient spectroscopy
E_C	Conduction band energy
E_d	Binding energy
EDX	Energy-dispersive X-ray spectroscopy
E_F	Fermi level
E_g	Band gap
$E_{g,d}$	Direct band gap
$E_{g,i}$	Indirect band gap
E_{max}	PL band position
E_V	Valence band energy
Φ	Integral intensity of a photoluminescence band
GaAs	Gallium arsenide
PCE	Power conversion efficiency
PL	Photoluminescence spectroscopy
PV	Photovoltaics
RTE	Rapid thermal evaporation
Sb_2O_3	Antimony oxide
Sb_2Se_3	Antimony selenide
SEM	Scanning electron microscopy
TDPL	Temperature-dependent photoluminescence
TDTS	Temperature-dependent transmission spectrum
VBM	Valence band maximum
VTD	Vapor transport deposition
XRD	X-Ray diffraction
α-Si	Amorphous silicon
σ (T)	Temperature dependent electrical conductivity

List of figures and tables

INTRODUCTION

It has been widely accepted that increasing the share of renewables in the production of electricity is of crucial importance for the processes of decarbonization. Among the pioneering renewable energy technologies over the last decades has been solar photovoltaics (PV). With an estimated cumulative installed capacity of 8519 GW by 2050, solar PV is expected to become one of the most prominent energy technologies next to wind energy [1]. In 2019, the global cumulative capacity of solar PV rose by 19%, reaching 633 GW in total with 117 GW of new capacity installed. Accounting for 2.7% of the global electricity supply, solar PV has the second-largest generation growth of all renewables. This places solar PV slightly behind wind energy and ahead of hydropower [2].

Crystalline silicon, an abundant material, has come to dominate the PV market. Despite its indirect band gap and poor absorption coefficient, it has been very successful from laboratory to commercial integration and it occupies, nowadays, 90% of the market's share. However, a wafer layer with a thickness of around 180 μm, which is conventionally used for PV module manufacturing, accounts for 50% of silicon (Si) solar cell production costs. This is a major concern, especially bearing in mind that crystalline Si PV has reached an unrivaled level of maturity both within the academy and industry. Precisely because of these, new PV technologies favoring more versatile applications and having less environmental footprint have been in the making for some time. Thin-film solar cells are among the new technologies attracting remarkable research and development focus as they enable low-cost production, high power conversion efficiency, and high specific power with an extremely lightweight and flexible structure [3]. Amorphous silicon (α-Si), cadmium telluride (CdTe), and copper indium gallium diselenide (CIGS) are the three most widely commercialized thin-film photovoltaics with a less than 10% market share. Each has a direct band gap and a strong light absorption capability, enabling the use of thin absorber material layer, usually in the range of 1-5 μm. When compared to CdTe and CIGS, α-Si does not only require a lower silicon content in comparison to crystalline silicon technologies. Since it does not use any toxic heavy metals such as cadmium (Cd) or tellurium (Te) or rare elements such as indium (In), tellurium and gallium (Ga), α-Si is also a more environmentally friendly option. However, CIGS and CdTe are more promising in terms of energy conversion efficiency as α-Si has a very high defect density. This leads to poor photoconductivity and prevents doping, both of which are undesirable properties for PV applications [4]. To date, CdTe and CIGS solar cells have been successful in achieving efficiencies of 22.1% and 23.4% [5], [6], respectively, while hydrogenated a-Si couldn't exceed 13.6 % [7]. Despite successful utilization of CdTe and CIGS absorbers in solar cells, their technologies remain behind crystalline silicon solar cell equivalents when it comes to efficiency and

reliability. In terms of efficiency and stability, CIGS solar cells are comparable to Si solar cells. However, the main issues of CIGS are lower yield, lower manufacturing capacity, higher module production cost, and faster performance degradation with time. Moreover, as already mentioned, the toxicity of Cd and Te, the scarcity and the high price of In, Ga and Te hinder the widespread use of CdTe and CIGS photovoltaics [8].

The chalcogenide antimony selenide (Sb_2Se_3) recently appeared as a promising alternative light-absorber material for high-efficiency photovoltaics because of its attractive structural, optical, and electrical properties and favorable environmental characteristics, such as a single-phase structure, suitable optical band gap (1.0 to 1.2 eV at 300 K), high light absorption coefficient (1×10^5 cm^{-1} at around 1.8 eV), low toxicity, and high element abundance [9]–[11]. In recent years, Sb_2Se_3-based solar cells have experienced rapid development. The highest reported efficiency of 9.2% was achieved by junction interface engineering of Sb_2Se_3 solar cells, which were fabricated by close-spaced sublimation (CSS) and in substrate configuration [12]. However, the reported record efficiency is still far from its theoretical maximum value of 32% [13] and is not yet competitive with thin-film solar cells on the market.

Achieving high efficiency for thin-film solar cells relies on our knowledge of semiconductor materials and interfaces. These include charge carrier transport mechanisms, recombination mechanisms, and impurities and defect structure [14]. The latter, namely the properties of impurities and native defects are crucial for controlling the material performance in PV devices. Defects are features in the crystal where the crystal symmetry is broken. In other words, defects are the products of impairment of the atomic arrangement from the ideal crystal structure. What defects do is to control the doping level of the material, carrier lifetime, and the rate of interfacial recombination [15]. One type of defect could make a semiconductor useful for producing a device, and yet another type might have negative impacts, rendering the device non-viable [16]. Usually, those defects possessing deeper energy levels and larger capture cross-sections tend to act as recombination centers which lead to low device efficiency [17]. Hence, it is of crucial importance to understand the properties of deep defect states inside the band gap for the future development of solar cell systems.

Photoluminescence (PL) is an optical and non-destructive method with very high sensitivity for studying recombination mechanisms and related defects in semiconductors. While low-temperature PL investigates the defect structure, temperature and laser power dependencies usually give information about the nature of recombination processes [18].

The present work is focused on the analysis of the defect structure of Sb_2Se_3 microcrystals by using photoluminescence spectroscopy. Recently, the energy levels of intrinsic defects have been determined by several experimental methods such as temperature-dependent electrical conductivity [19], [20], admittance spectroscopy [11], [19], and deep level transient spectroscopy [21], [15]. These empirical works are followed by theoretical calculations using density functional theory [17], [22]. However, the photoluminescence method as one of the most sensitive tools for studying defects and related recombination mechanisms in semiconductors is barely used for defect studies of Sb_2Se_3. In consideration of previously determined energy levels and their assigned defects, this thesis aims to deliver a detailed analysis of the PL spectra of Sb_2Se_3 microcrystals and to reveal the radiative recombination mechanisms and related defects.

The organization of this thesis is following; it consists of three main chapters. At first, the literature review introduces Sb_2Se_3 as absorber material for solar cells, including its defect structure. In addition, the main material characterization technique, photoluminescence spectroscopy is introduced. Following the literature review, the experimental part describes the synthesis of Sb_2Se_3 microcrystals and the experimental setups of characterization techniques. The main part of the thesis is dedicated to results and discussion focusing on the analysis of the temperature and laser power-dependent photoluminescence spectra of studied Sb_2Se_3 microcrystals. A radiative recombination model for the studied materials is presented. Finally, the conclusions and outlook wrap up the thesis.

1. LITERATURE REVIEW

1.1 Antimony selenide (Sb_2Se_3) absorber material for solar cells

1.1.1 General description of Sb_2Se_3

Sb_2Se_3 is a very promising photovoltaic absorber material because of its attractive structural, optical, and electrical properties [9] and favorable environmental characteristics [23]. Antimony selenide has a one-dimensional crystal structure comprising of covalently bonded $(Sb_4Se_6)_n$ ribbons stacking together through van der Waals force (see Figure 1.1). This special structure results in anisotropic optical and electrical properties [12]. Sb_2Se_3 is a stable chalcogenide [24] and it belongs to the family of inorganic binary V_2-VI_3 compounds [25]. It has a simple binary composition with a fixed orthorhombic phase. The only expected secondary phases are elemental selenium (amorphous or trigonal), elemental antimony, and antimony oxide (Sb_2O_3), which can be detrimental to the overall performance of the solar cells [26]. Sb_2Se_3 has lattice constants of a = 11.62 ± 0.01, b = 3.96 ± 0.01 Å, and c = 11.77 ± 0.0 Å with a primitive cell volume of 0.524 nm^{-3} and density of 5810 kg/m^3 [27]. The raw materials antimony (Sb) and selenium (Se) are comparatively abundant, low-toxic, and low-cost. The abundance of Sb and Se elements in the Earth's crust is 0.2 and 0.05 ppm, respectively. Sb_2Se_3 is not on the lists of highly toxic materials by American, European Union, or Chinese regulation authorities, nor in the lethal dose LD50 or lethal concentration LCt50 data [23]. As a consequence of the low buying rates, the cost of the raw material is only 5 cents for depositing a 1 m^2 Sb_2Se_3 thin film at a film thickness of 1 μm [25]. Fabrication costs are also reduced due to a binary elemental composition, single-phase, and low-temperature deposition (low melting point of 885 K) [24]. The theoretical absorption coefficient was found to be $>1 \times 10^4$ cm^{-1} for energies above 1.5 eV, increasing to 1×10^5 cm^{-1} at 1.8 eV, indicating a sharp and strong absorption edge [28]. As a result, Sb_2Se_3 films with only 1 μm thickness are sufficient to absorb photons within the wavelength range of 400–1100 nm, which is an almost optimal spectral range for PV conversion [9]. Thin-film Sb_2Se_3 normally exhibits p-type conductivity [10]. Its electron mobility is 15 $cm^2V^{-1}s^{-1}$, and the hole mobility is 42 $cm^2V^{-1}s^{-1}$, comparable with that of CdTe (μ_p = 60 $cm^2V^{-1}s^{-1}$). Furthermore, its dielectric constant is relatively larger compared with CIGS (ε = 13.6) and CdTe (ε = 7.1), which leads to a lower exciton binding energy that implies an immediate separation of electrons and holes upon photogeneration [25].

Sb_2Se_3 can be characterized as a near-direct band gap material. For Sb_2Se_3 single crystals and polycrystalline thin films, both direct and indirect transition types with band

gap (E_g) ranging from 1.0 to 1.3 eV (T=300 K) were reported [9], which approaches the ideal Shockley-Queisser value [11]. Amorphous antimony selenide (a-Sb_2Se_3) has a larger gap than crystalline antimony selenide (c-Sb_2Se_3). The energetic difference between the indirect and direct band gap of Sb_2Se_3 decreases towards lower temperatures and was found to be only 0.04 eV at T = 0K [10].

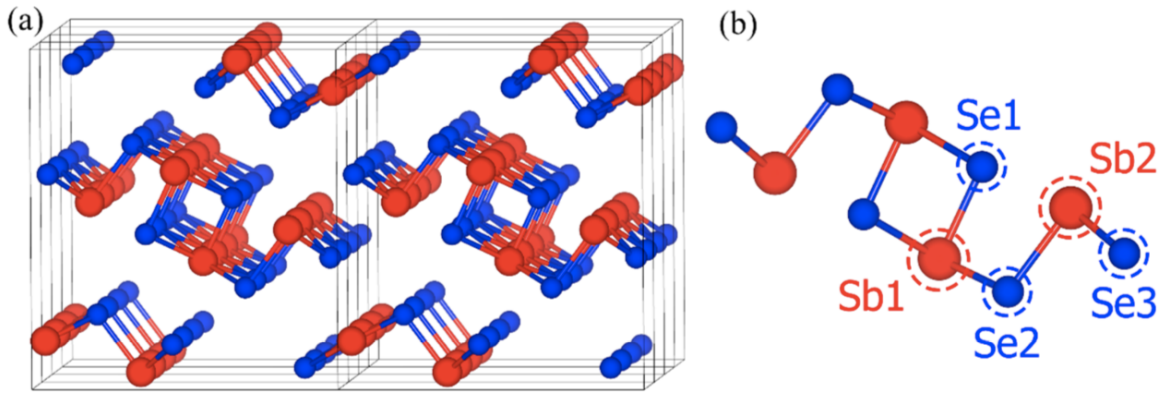

Figure 1.1: (a) Crystal structure of Sb_2Se_3 and (b) the non-equivalent atomic sites in each $[Sb_4Se_6]_n$ atomic chain. Two Sb sites and three Se sites are shown in red and blue, respectively [29].

1.1.2 Sb_2Se_3 photovoltaic devices over the time

Sb_2Se_3 based PV devices have only progressed recently, with the first report of a notable efficiency being 3.21% by Choi et al. [30]. Since then, progress has been rapid, reaching 5.6% for a CdS/Sb_2Se_3 heterojunction in 2016 [31] and, more recently, 5.9% for a ZnO/Sb_2Se_3 heterojunction [32], and the next record 7.6% for CdS/Sb_2Se_3 [21]. Despite its short development time, Sb_2Se_3 has already surpassed the efficiencies of long-investigated binary inorganics, such as tin sulfide (SnS) and iron disulfide (FeS_2) [28]. An efficiency of 9.2%, which is the highest value reported so far for this type of solar cells, is achieved by junction interface engineering [12].

Most of these champion cells were prepared by using rapid thermal evaporation (RTE), except the one with 7.6%, which was prepared by vapor transport deposition (VTD) [21]. Very recently, Li et al. [12] reported on Sb_2Se_3 solar cells fabricated by CSS method with a power conversion efficiency (PCE) of 9.2%. To date, devices prepared using physical deposition methods exhibited higher performance than chemical deposition methods. It has been reported that Sb_2Se_3 solar cells can be fabricated using both substrate and superstate configurations. Nevertheless, the superstrate configuration has been used more extensively in most of the champion solar cells [32],

[34], [35], [32], [21], [31]; except for the latest 9.2% champion device, which was fabricated in substrate configuration [12].

Despite the rapid improvement, the PCE is still far behind conventional CIGS (PCE = 23.4%), CdTe (PCE = 22.1%), copper zinc tin sulfoselenide (CZTSSe) (PCE = 12.6%), and even α-Si (PCE = 13.6%) solar cells [19]. Mavlonov et al. [27] reported that in the future, the following factors should be considered to further improve the PCE of Sb_2Se_3 solar cells: enhancement of the photocurrent, improvement of the open-circuit voltage and fill factor via optimized carrier management, systematic investigation of defects, implementation of novel buffer layers, optimization of device fabrication. However, the study on Sb_2Se_3 is lacking because of two difficulties: (1) the intrinsically low electrical conductivity (10^{-6} – 10^{-7} $S.cm^{-1}$) of Sb_2Se_3 film creates obstacles for obtaining carrier density and mobility directly from Hall effect measurement; (2) the strong anisotropy in Sb_2Se_3 crystal renders mobility measurement very complicated. Nevertheless, understanding fundamental parameters of thin-film Sb_2Se_3 is of great importance to device configuration design, performance, and optimization [19].

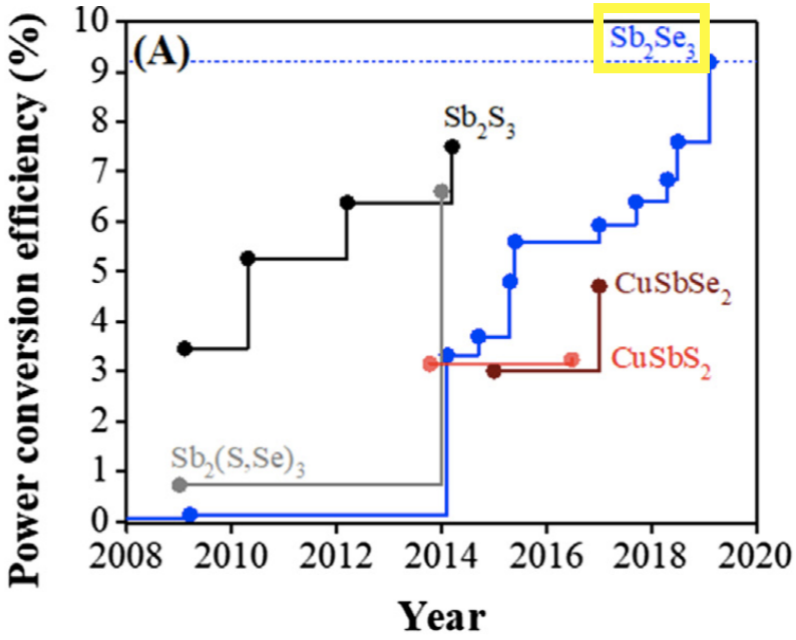

Figure 1.2: The record PCEs for Sb-related thin-film solar cells: Sb_2Se_3 (blue) [27].

1.1.3 Optical properties

The optical properties of Sb-Se compounds strongly depend on both crystal structure and chemical composition [27]. Polycrystalline Sb_2Se_3 films with stoichiometric composition exhibit E_g within the range of 1.0–1.3 eV in most of the reports [9], [35], [12]. This E_g variation in polycrystalline films was attributed to the fact that Sb_2Se_3 thin films prepared by various methods and growth conditions could have different Sb/Se ratios and/or different crystalline quality [13].

Chen et al. [9] confirmed optical transition type of c-Sb_2Se_3 by the temperature-dependent transmission spectrum (TDTS) and temperature-dependent photoluminescence (TDPL). It is found that c-Sb_2Se_3 is an intrinsically indirect band gap ($E_{g,i}$) material with the lowest $E_{g,i}$ of 1.03 ± 0.01 eV and the lowest direct band gap ($E_{g,d}$) of 1.17 ± 0.02 eV at 300 K which indicates a small energy difference. At temperature above 150 K, both direct and indirect transitions contribute to film absorption, while at temperature below 150 K, the only contribution is from direct band gap [9].

It is reflected by experimental data, that Sb_2Se_3 films have a high absorption coefficient in the range of 10^5 cm^{-1} for photon energies higher than the band gap [36], [23], [9]. This is a proof that Sb_2Se_3 can be granted as a suitable absorber material for high-efficiency thin film solar cells. A higher absorption coefficient enables fabricating thinner absorber layers. While the incident light with photons below 800 nm wavelength is entirely absorbed within 400 nm thick film, the penetration depth for photons with wavelength beyond 900 nm reaches a micron.

The dielectric constant related to dielectric polarization and exciton binding energy is also an essential parameter in semiconductors. The complex relative dielectric constant could be described as $\varepsilon' = n^2 - k^2$, $\varepsilon'' = 2nk$, where ε' and ε'' are the real and imaginary parts of the complex relative dielectric constant; n and k are the refraction index and the extinction coefficient, respectively. ε' ranged from 10.7 to 16.5 at 612 – 1693 nm for a-Sb_2Se_3 and 14.3 to 19.8 at 852 – 1693 nm for c-Sb_2Se_3 [9]. High dielectric constant values are favorable for the absorber layer because they lead to better screening of the photo-generated charge carriers from electrically charged defects. Compared with CIGS, CdTe and copper indium diselenide (CIS); the larger dielectric constant of c-Sb_2Se_3 suggests smaller exciton binding energy and possibly immediate separation of electrons and holes upon photogeneration [27].

1.2 Defects in semiconductors

1.2.1 Classification of defects

Defects are defined as imperfections in a perfect crystal. In practice, all crystals have impurities, whether by design or by accident and they have control over the doping level of the material, carrier lifetime, and the rate of bulk and interfacial recombination. To improve the performance of a solar cell, a proper understanding of its defect properties is of crucial importance. The incorporation of electrically active dopants enables modifying the electrical properties of semiconductors. When an impurity is intentionally introduced into a semiconductor, then it is defined as a dopant. In addition, all semiconductors contain native defects. Our expertise to control different types of defects is highly decisive for the use of semiconductors in device applications [16], [37].

Defects can be classified by their atomic structure or by the energy levels that they introduce into the band gap. Starting with the energy levels, defects can be divided into two wide categories. Impurities whose electronic energies can be calculated using the "effective mass approximation" are referred to as shallow impurities. Defects whose energies cannot be calculated with that approximation are known as deep centers. Early on, the deep levels were defined as energy levels, which are located near the middle of the band gap, and the shallow levels as the ones located near the band edges. However, now it is discovered that many defects with energy levels in the band gap near the corresponding band edge have similar properties to deep levels and can act as traps for the photoinduced charge carriers. As a result, the term "deep level" has been broadened to any center, which cannot be classified as shallow [16].

According to their atomic structure, defects can be either a point defect, a line defect, or three-dimensional bulk defects such as precipitates of secondary phase. Point defects can also form defect pairs and complexes. A point defect usually occurs in a specific location in the crystal that involves isolated atoms. Line defects involve rows of atoms with a typical example of dislocations. Lastly, there are complexes that are formed from a small number of point defects. Line defects are usually detrimental to devices, therefore they have to be passivated. However, since the properties of point defects and defect complexes tend to determine the electronic and optical properties of a semiconductor, attention must be focused on them. Isolated point defects are further classified as follows:

Vacancy: the vacancy created by a missing atom A is denoted by V_A.

Interstitial: an atom A occupying an interstitial site is denoted by A_i.

Substitutional: an atom C replacing a host atom A is denoted by C_A.

Antisite: a special kind of substitutional defect in which a host atom B occupies the site of another host atom A, also denoted as substitutional defect B_A.

Frenkel defect pair: a complex V_A+A_i formed by an atom A displaced from a lattice site to a nearby interstitial site forming a charge neutral defect pair [16].

The Schottky defect pair: a complex V_A+V_B formed by two oppositely charged host atom vacancies maintaining charge neutrality and stoichiometry [37].

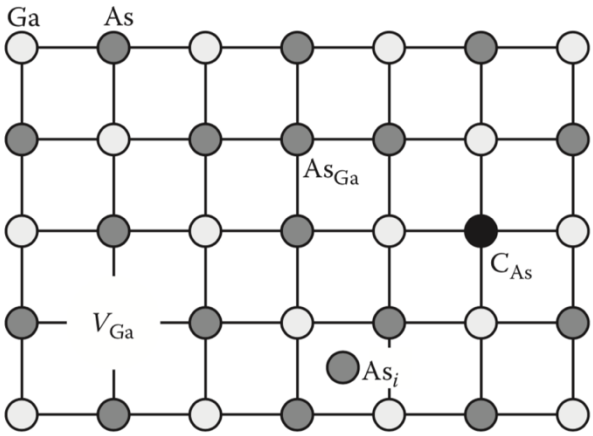

Figure 1.3: Defects in gallium arsenide (GaAs): gallium vacancy (V_{Ga}), arsenic interstitial (As_i), arsenic antisite (As_{Ga}), and substitutional carbon (C_{As}) [37].

In addition to forming a defect pair, defects can also form complexes involving more than two defects. Vacancies, interstitials and antisite defects are intrinsic or native defects since they only involve the atoms of the host crystal. When defects involve foreign atoms (i. e., impurity atoms), then these are referred to as extrinsic defects [16].

Many defects are electrically active and they can introduce electronic levels into the band gap. These energy levels are basically the reason why semiconductors have gained huge importance. Defects that can contribute free electrons to the host crystal are known as donors. A donor level is one where the center becomes positively charged when it gives up its electron. Defects that can contribute holes (i. e., remove free electrons) are known as acceptors. An acceptor level is negative when occupied by an electron. In general, semiconductors contain a mix of donors and acceptors. If a semiconductor contains more donors than acceptors, for instance, then all of the acceptors will be negatively ionized to compensate the donors.

For a donor impurity, the energy difference between the conduction band minimum (CBM) and the donor level is the ionization energy or binding energy (E_d). This is the amount of energy required to excite an electron from the donor atom into the conduction

band. A donor is neutral when it has an electron bound to it and is positive when the electron is liberated. The donor level is therefore called the (0/+) level. For an intrinsic semiconductor, the Fermi level (E_F) is near the middle of the band gap. If the E_F is above the (0/+) level, then the level is occupied, so the donor is neutral. When the E_F is below the (0/+) level, the level is unoccupied, and the donor has a charge of +1. The other way around, an acceptor level is called the (0/−) level. When the Fermi level is above the (0/−) level, then the acceptor has a charge of −1. When the E_F is below the (0/−) level, the level is unoccupied so the acceptor is neutral [37].

1.2.2 Defect structure of Sb_2Se_3

The formation of defects accelerates radiative and nonradiative recombination and degrades device performance [21]. Several researchers have experimentally investigated intrinsic defects in Sb_2Se_3 using admittance spectroscopy (AS) [19], [11], temperature-dependent electrical conductivity (σ(T)) [19], [20], deep level transient spectroscopy (DLTS) [21], [15], and photoluminescence spectroscopy [10], [38], [39], [23]. Experimentally determined energy levels of intrinsic defects in Sb_2Se_3 are summarized in in Table 1.1.

From DC reverse bias-dependent admittance measurements Hu et al. [11] found that the capacitance response was indicating to three defect levels in the band gap of Sb_2Se_3 that were named D1 (0.286 eV above VBM), D2 (0.188 eV above VBM), and D3 (0.570 eV above VBM). Although the capture cross-section of D1 was large, the defect density was low and the capture lifetime of holes was in the order of microseconds, suggesting that D1 may not act as an effective trapping center. D2 was assigned as a shallow acceptor level since the capture cross-section was so small and had a long capture lifetime of holes in the order of milliseconds. D3 with both, high defect density and large capture cross-section had a very short capture lifetime of holes in the order of nanoseconds and, therefore, may act as very effective trapping or recombination center that limits the efficiency of the Sb_2Se_3 solar cell. However, the activation energy and the capture lifetime of holes of both, D1 and D2 somehow related to cell efficiency, while no obvious relationship was found between D3 and efficiency. Both D1 and D2 were identified as bulk-type defects, while D3 was identified as an interface or near-interface defect [11]. The bulk defects were not assigned to specific defects in Sb_2Se_3.

Chen et al. [19] reported about the temperature dependent conductivity and AS measurements that were applied to determine the depth and density of defect states in thin film Sb_2Se_3, respectively. From the temperature-dependent conductivity measurements in between 160 K and 250 K a defect with an ionization energy of 0.111

eV was found. This defect is ascribed to the shallow acceptor defect of Se_{Sb}. AS was used to determine the density of defect states and there was a Gaussian defect peak in the gap with the peak position at 0.095±0.008 eV, which is consistent with the defect depth of 0.111±0.005 eV obtained from temperature dependent conductivity measurement. Moreover, H. Deng et al. [20] conducted temperature-dependent electrical conductivity measurements as well and found out that for the Se-rich $Sb_2(Se_xS_{1-x})_3$ alloy, the film only had one kind of shallow defect at 0.06 eV above valence band maximum (VBM) attributed to Se_{Sb}, which played little effect to photocarrier recombination.

Wen et al. [21] subsequently investigated the deep defects in CdS/Sb_2Se_3 solar cells fabricated via VTD. DLTS was used to investigate defect energy level, type, and concentrations. Two acceptor defects were found, H1 at 0.48 eV above VBM and H2 at 0.71 eV above VBM, which were attributed to V_{Sb} and Se_{Sb}, respectively. In the same study, a donor defect at 0.61 eV below CBM attributed to Sb_{Se} was also found. It is also shown, that Se_{Sb} and Sb_{Se} acceptor and donor defects always have similar densities with each other. This indicates that antisite defect pairs are formed in Sb_2Se_3 films, presumably forming a [Sb_{Se} + Se_{Sb}] complex [21]. Another DLTS study is presented by Hobson et al. [15], where both Sb_2Se_3 bulk crystals and solar cells were investigated. The three defects were named as E1, E2, and E3, which are corresponding to energy levels 0.378, 0.460, and 0.690 eV below the CBM, respectively. All the results show common deep level signatures and they are expected to strongly limit the performance of the solar cell. However, E3 has been consistently found as a problematic mid-gap and as the dominant defect level [15].

Grossberg et al. [10] presented a PL study for investigating recombination mechanisms and related defects in Sb_2Se_3 polycrystals. Three PL bands positioned at 1.24 eV (PL1), 1.10 eV (PL2) and 0.94 eV (PL3). Temperature and laser power dependent photoluminescence spectroscopy revealed the origin for the detected PL bands at 1.24 eV and 0.94 eV as donor-acceptor pair (DAP) recombination. The PL1 band involves more distant DAPs while the PL3 band results from the deep donor-deep acceptor (DD-DA) pair recombination. PL2 band at 1.10 eV is proposed to originate from a recombination related to the grain boundaries [10]. Recently, Krustok et al. [38] presented a detailed study of free exciton and biexciton emissions in Sb_2Se_3 microcrystals under high photoluminescence excitation density. The A free exciton peak was found at 1.311 eV and the B free exciton peak at 1.333 eV. The A and B biexcitons were detected at 1.302 eV and 1.322 eV, respectively. According to peak positions of observed free exciton and biexciton peaks from both, A and B band gaps at T = 3 K, the binding energies of the excitons were calculated as 9 and 11 meV for B and A biexcitons, respectively, and 6 meV for the A free exciton [38]. Shongalova et al.[39] and Zhou et

al. [23] also reported measured PL spectra. However, there is no analysis of the data presented to the reader. While Shongalova et al. detected the presence of two broad (~100 meV) deep PL bands at 0.75 eV and 0.85 eV at T = 7 K, Zhou et al. [23] measured a PL peak which is asymmetric with its peak located at 1.11 eV. The asymmetric shape of the PL bands referred to the presence of randomly distributed crystalline defects or impurities in the material.

Table 1.1: Experimentally determined energy levels of intrinsic defects in Sb_2Se_3.

Energy level (meV)	Proposed defect	Method	Reference
E_V + 111 meV	Se_{Sb}	σ (T)	[19]
E_V + 95 meV	Se_{Sb}	AS	[19]
E_V + 480 meV	V_{Sb}	DLTS	[21]
E_V + 710 meV	Se_{Sb}	DLTS	[21]
E_C – 610 meV	Sb_{Se}	DLTS	[21]
E_V + 286 meV	-	AS	[11]
E_V + 188 meV	-	AS	[11]
E_V + 60 meV	Se_{Sb}	σ (T)	[20]
E_C – 378 meV	-	DLTS	[15]
E_C – 460 meV	-	DLTS	[15]
E_C – 690 meV	-	DLTS	[15]
E_C – 47 meV	Sb_{Se}	PL	[10]
E_C – 285 meV	Sb_{Se}	PL	[10]
E_V + 33 meV	V_{Sb}	PL	[10]
E_V + 65 meV	V_{Sb} or Se_{Sb}	PL	[10]
E_V + 95 meV	Se_{Sb}	PL	[10]
E_C – 11 meV	-	PL	[38]
E_C – 6 meV	-	PL	[38]
E_C – 9 meV	-	PL	[38]

On the other hand, Liu et al. [17] and Savory et al. [22] have performed theoretical defect calculations using density functional theory. The simulations revealed two detrimental donor defects, V_{Se} and Sb_{Se}, easily forming under the Se-poor condition, while the more benign defects, Se_{Sb} and Se_i, are the dominant defects in Sb_2Se_3 film produced in an Se-rich environment [17]. By the ab initio calculation, it is also predicted that V_{Sb} and Se_{Sb} are dominant acceptor defects in Se-rich Sb_2Se_3 contributing to the p-type conductivity [29], [28], [23].

Theoretical studies showed that under Sb-rich conditions several defects e.g., V_{Se}, Sb_{Se} and the Se_i, have formation energies below 1.5 eV, and are therefore expected to be present in the film in reasonable concentrations (Figure 1.4a). However, under Se-rich condition, the formation energies of several problematic defects are moved to higher energy positions (Figure 1.4b). Overall, studies have shown that harmful intrinsic defects have lower concentration under Se-rich condition compared to Sb-rich condition. Therefore, it is predicted that longer minority carrier lifetime, better p-type conductivity, and thus much better PV efficiency can be achieved under the Se-rich condition [17], [22].

Liu et al. [17] showed that compared with the donor defects V_{Se} and Sb_{Se}, the acceptor defect Se_{Sb} has much lower formation energy and thus higher concentration, which makes the sample show intrinsic p-type conductivity [17]. V_{Se} was reported to act not only as n-type donor that reduces the effective p-type doping density of Sb_2Se_3 film, but also as a recombination center trapping photogenerated carriers [25].

Although the antisite defects Sb_{Se} and Se_{Sb} usually have an insignificant concentration in three-dimensional covalent semiconductors, their concentration in Sb_2Se_3 is high. Similarly, the anion interstitial defect Se_i has a high concentration in Sb_2Se_3 due to low defect formation energy. As can be seen from Figure 1.5, Se_i has the (-2/0) ionization level above the CBM, which means it does not contribute to the carrier concentration or act as nonradiative recombination center. Consequently, it does not induce any deep level in the band gap and its influence on the PV performance is benign [17].

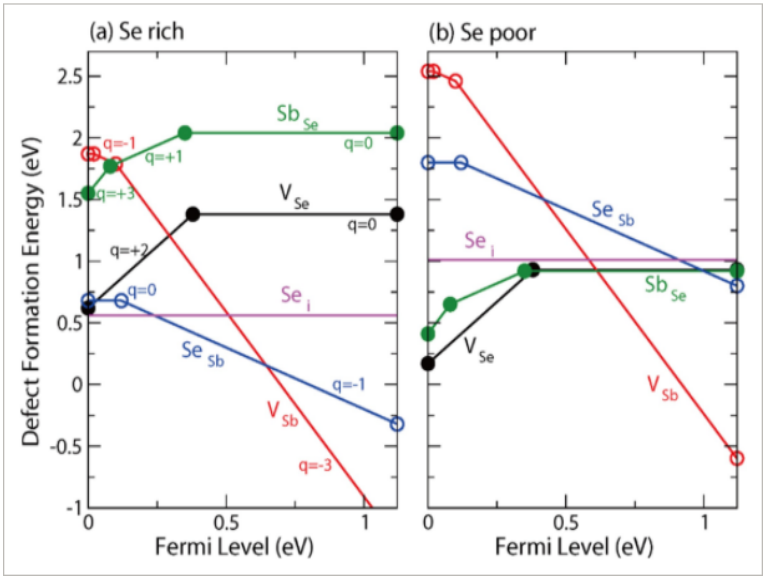

Figure 1.4: The calculated formation energies of point defects in Sb_2Se_3 as a function of the Fermi level under a) Se-rich condition and b) Se-poor condition. q shows the charge states of the ionized defects, with positive q showing ionized donor and negative q showing ionized acceptor defects [17].

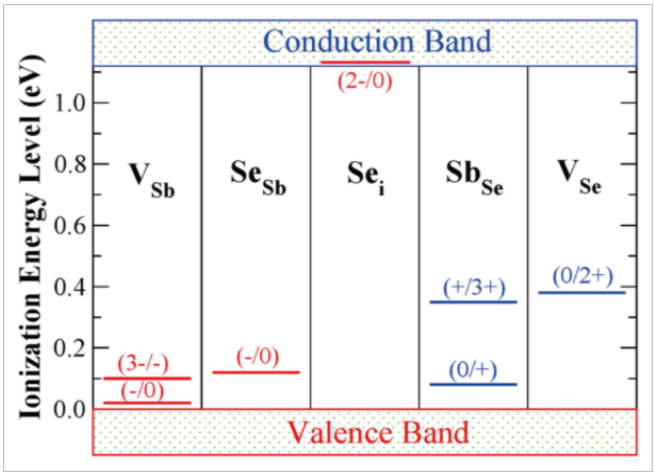

Figure 1.5: The ionization energy levels of point defects in Sb_2Se_3, referenced to the VBM level. The red lines show the acceptor levels, and the blue lines show the donor levels [17].

1.3 Photoluminescence spectroscopy

1.3.1 Theory of photoluminescence

Photoluminescence is a non-destructive and highly sensitive optical technique used for the determination of the electronic structure of semiconductors, including defect energy levels. By definition, photoluminescence is the optical radiation emitted by a physical system (in excess of the thermal equilibrium blackbody radiation) resulting from excitation to a non-equilibrium state by irradiation with light [40]. The method enables detecting the defects including their type, ionization energy, etc., determining the band gap energy, the phase composition, and dominating radiative recombination mechanisms. As a research tool, PL has the advantage of simplicity regarding sample preparation. Also, materials from bulk crystals to thin films can be studied. However, the information gained from the PL experiment requires very often detailed and complicated analysis. For this reason, to assign the PL features to physical phenomena correctly, usually many spectra of the same sample are measured with various temperatures as well as laser excitation powers [41].

The photoluminescence process includes three main phases, which are (1) excitation, (2) thermalization and (3) recombination. In the first event, the crystal is irradiated with photons of energy greater than the band gap energy of the material. Consequently, the electrons are promoted to higher energy levels in the conduction band, resulting in the creation of electron-hole pairs. Then, excited pairs relax towards quasi-thermal equilibrium distributions, where the excess energy of the electron is given to the crystal lattice and the electron relaxes to the bottom of the conduction band [42]. During the third event, the recombination of an electron and a hole takes place and this

recombination energy will transform into radiative emission. As a result of a radiative recombination, a photon is emitted with energy always smaller than the energy of the exciting photon [41]. A PL spectrum, therefore, contains information about the recombination mechanisms of photoexcited charge carriers in the material [43].

Temperature dependence

The PL peak position shift and the decline of the peak integral intensity Φ with increasing temperature indicates to a specific recombination process. If the PL peak shift is following the temperature dependence of the band gap energy, then this is an indication of the involvement of the band states in the recombination process [10]. In other cases, DAP recombination, recombination involving fluctuating potentials, grain boundaries etc. have to be considered. The ionization energies of the defect levels participating in the recombination process can be determined from the temperature dependence of the PL spectrum [44]. The thermal activation energies for the PL bands are obtained from the Arrhenius plot where the dependence of ln Φ(T) versus 1000/T at high temperatures is fitted by using theoretical expression for discrete energy level [45]:

$$\Phi\,(T) = \frac{\Phi\,(0)}{1+\alpha_1 T^{3/2}+\alpha_2 T^{3/2} exp\,(-E_T/kT)}, \qquad (1.1)$$

where α_1 and α_2 are the process rate parameters and E_T is the thermal activation energy.

Laser power dependence

Different processes result in different contributions to the luminescence spectrum with increasing excitation laser power [45]. The shift of the PL band position with changing laser power may originate from various processes. Among the most probable are (1) potential fluctuations in compensated samples, (2) impurity band formation, and (3) changes in the DAP-type emission due to differences in the recombination probabilities of close and distant pairs [46].

Additional information about the type of recombination process can be obtained from the laser power dependence of the PL band integral intensity Φ. The dependence can be described as $\Phi \sim P^k$, where P is the laser power. The k value, which can be obtained from the $\Phi\,(P)$ plot on the log-log scale, is an indication of the type of recombination. For defect related recombination $k < 1$ is obtained, $k \geq 1$ indicates to a band-to-band or excitonic emission [47].

1.3.2 Recombination mechanisms

At thermal equilibrium, the carrier population decreases exponentially with energy and therefore emissions are strongest from the lowest energy states. If there are defect levels inside the band gap, the photoexcited electrons and holes can recombine radiatively at these energy levels. This recombination can be either radiative (release of a photon) or non-radiative (no photon production). When a spontaneous emission is produced, the defect can be defined as a radiative recombination center and the energy of the emitted photon is dependent on the change in the energy state of the electron-crystal system. The amount of emission produced by a body under thermal equilibrium at room temperature is very small, therefore most experiments are carried out under nonequilibrium conditions. The creation of such conditions and the detection of the resultant spontaneous emission from the sample is the essence of luminescence experiments [16].

The traps which can act as recombination centers for electronic transition within the band gap are either donor or acceptor levels. By studying the nature of these defect levels, information about the impurity or defect can be resolved. Figure 1.6 represents the energy band diagram of a semiconductor, illustrating the most common radiative transitions. These transitions are excitonic transition, donor–acceptor pair transition, free-to-bound transition (either band to acceptor or donor to band), and band-to-band transition [42]. The properties of each recombination channel are different, especially their behavior with temperature and laser power, which is why temperature and excitation power dependent PL measurements are needed to identify the type of recombination. There are some specific features of each type of PL emission and the relevant ones for this thesis are described in the next sections.

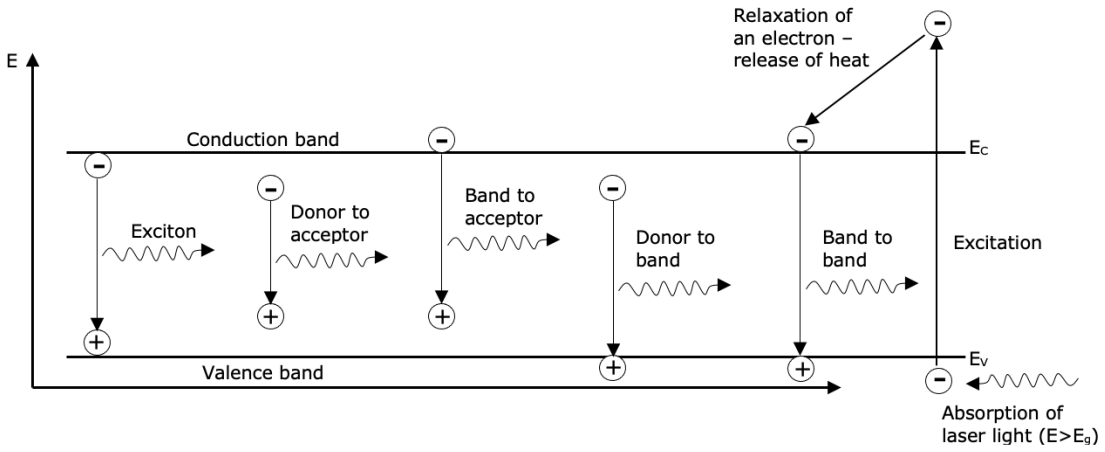

Figure 1.6: Most common radiative transitions observable with photoluminescence spectroscopy [41].

1.3.2.1 Donor-acceptor pair recombination

Often a semiconductor contains both donor and acceptor impurities. Under illumination, electrons and holes can be trapped forming neutral donors (D^0) and neutral acceptors (A^0) at the sites of ionized donors (D^+) and ionized acceptors (A^-). When returning to equilibrium, some of the electrons on the neutral donors will recombine radiatively with holes on the neutral acceptors. This process is known as a donor–acceptor pair transition (DAP transition) and can be represented by the reaction [16]:

$$D^0 + A^0 \rightarrow E_{DA} = D^+ + A^-. \quad (1.2)$$

The emission energy from a DAP separated by a distance R (R is much larger than the lattice constant) can be calculated by the following equation, where Coulomb interaction between the donors and acceptors modifies the DAP binding energy in such a way that the transition energy E_{DA} is distance-dependent [42].

$$E_{DA} = E_g - (E_A + E_D) + \left(\frac{e^2}{4\pi\varepsilon_0\varepsilon R}\right), \quad (1.3)$$

where E_g is the band gap energy, E_A and E_D are the acceptor and donor ionization energies, respectively, e is the electron charge, ε is the static dielectric constant, and ε_0 is the permittivity of vacuum. The last term of Eq. (1.3) describes the Coulomb interaction between the donor and acceptor defects [16]. As excitation power density increases, the recombination involving more distant DAPs saturates and mainly closer pairs having stronger Coulomb-interaction energy dominate the recombination. Therefore, PL emission resulting from the DAP recombination shows energy shift to higher energy side when the excitation power density is increased (so-called blueshift) and this energy shift is a feature of DAP recombination process [44]. It is important to notice that the magnitude of the blueshift is usually in the order of few meV per decade of laser power density.

However, the correct value for the dielectric constant ε in the case of very close pairs is quite difficult to calculate, because it is obvious, that in compound semiconductors ε must be a combination of both optical and static dielectric constants. Therefore, Eq. (1.3) must be considered as a very rough method to calculate the transition energy of close donor-acceptor pairs. For very close pairs, where $R_1 \approx R_2$ (shortest and the next shortest donor-acceptor distance respectively), the energy separation ΔE between the donor-acceptor pairs of the nearest or the next-nearest neighbors can be calculated as follows [48]:

$$E_{DA} = \left(\frac{e^2}{\varepsilon}\right)\left(\left(\frac{1}{R_1}\right) - \left(\frac{1}{R_2}\right)\right). \quad (1.4)$$

1.3.2.2 Free-to-bound recombination

At high temperatures, the shallow defects are expected to ionize and therefore band-to-band recombination dominates. However, at lower temperatures, where the thermal energy of carriers is smaller than the ionization energy of the defects, a free electron in the conduction band can recombine with the holes trapped on the acceptors, or holes in the valence band can recombine with the electrons trapped on the donors. This kind of transition is called free-to-bound recombination. The emitted photon energy, i.e., the peak position of the PL band E_{max} resulting from a free-to-bound recombination involving an acceptor defect is described as:

$$E_{max} = E_g - E_A \tag{1.5}$$

where E_g is the band gap energy and E_A is the acceptor binding energy. The equation can be formulated for the donor to band transition with using the donor binding energy E_D instead of E_A as well [16].

If the temperature dependence of the PL band position follows the temperature dependence of the band gap and if the PL band position does not shift with the varied laser excitation power, then this is an indication that the band states are involved in the recombination process [10]. If in addition, the laser power dependence of the integrated intensity of the PL band Φ follows the $\Phi \sim P^k$ (P is laser power) relation with k<1, then this PL band originates from the free-to-bound recombination.

1.3.2.3 Excitonic recombination

Excitons are expected to form when photoexcited electrons and holes are bound to each other by Coulomb interaction [16]. An exciton (also called a free exciton) is the fundamental electronic excitation in a semiconductor, yet it may become trapped at defect sites before the electron-hole pair recombines [49]. At low temperatures, the neutral donor and acceptor defects attract excitons via van der Waals interaction, and eventually the defect bound excitons form. Free excitons can also be bound to each other forming a biexciton. Excitons are most often investigated by low-temperature PL spectroscopy on high purity and high-quality semiconductors [16].

PL emission resulting from a free exciton is usually situated very close to the band gap energy and follows its temperature dependence. Moreover, the laser power dependence of the integrated PL intensity shows a linear growth, where the coefficient k is expected to be $k > 1$. The biexciton, on the other hand, shows a remarkable red-shift with the increasing temperature and the integrated intensity shows a superlinear growth with the increasing laser power with $k \approx 2$ [38].

Aim of the thesis

In the literature, Sb_2Se_3 is presented as a promising photovoltaic absorber material due to its high absorption coefficient [28], near-direct optimal band gap [9], and its rapid improvement in the last decade [12]. Yet, further progress can only be achieved with optimized carrier management, implementation of novel buffer layers, optimization of device fabrication, and systematic investigation of defects [27]. This thesis focuses on understanding the properties of intrinsic defects in Sb_2Se_3 using photoluminescence spectroscopy. As can be seen from the literature review, only a few researchers have investigated the defect structure of Sb_2Se_3. Moreover, PL owns a very small share among the characterization methods used for studying the defects in this material. The theoretical simulations based on the density functional theory reveal that V_{Se} and Sb_{Se} are two detrimental donor defects in Sb_2Se_3 produced in a Se-poor environment, while Se_{Sb} and Se_i are more benign defects in Sb_2Se_3 produced in a Se-rich environment [17]. However, the common result from theoretical calculations and experimental methods demonstrates that cation-anion antisite defects (Se_{Sb} and Sb_{Se}) are the dominant defects, making them the most likely candidates for possible recombination centers. Moreover, these antisite defect pairs formed in Sb_2Se_3 films also presumably form [Sb_{Se}+Se_{Sb}] defect complexes [17], [22].

When the above-given information is taken into consideration, the present study aims:

1. To familiarize with the main material characterization techniques (PL and Raman spectroscopy) used in thesis.

2. To investigate the intrinsic defects in Sb_2Se_3 microcrystals with different elemental compositions using PL spectroscopy.

3. To clarify the main radiative recombination processes in examined Sb-rich and stoichiometric Sb_2Se_3 microcrystals.

2. EXPERIMENTAL

2.1 Synthesis of Sb_2Se_3 microcrystals

The two Sb_2Se_3 samples, Sb-rich and stoichiometric Sb_2Se_3 studied in this thesis consisted of several randomly oriented microcrystals that mostly had a needle-like shape and the size of couple of tenths of micrometers in width and up to hundred micrometers in length, see scanning electron microscopy (SEM) images in Figure 2.1.

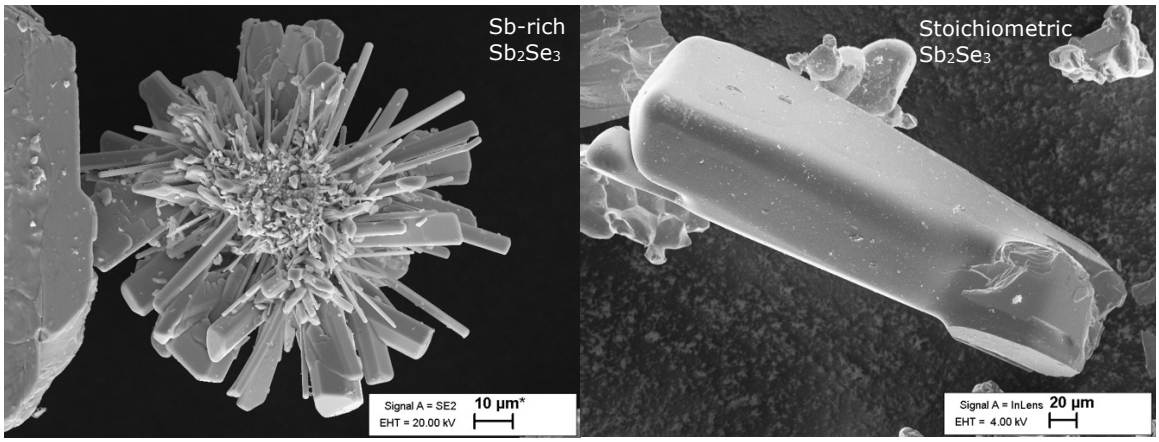

Figure 2.1: SEM images of Sb-rich and stoichiometric Sb_2Se_3 microcrystalline powders synthesized at temperatures 380ºC (left) and 450ºC (right).

The Sb_2Se_3 microcrystalline powders were synthesized in a two-temperature zone furnace in the sealed evacuated quartz ampoules from 5N purity Sb metal powder and elemental Se pellets with 4N purity. Sb metal powder (0.1 g) was poured into one side of a quartz ampoule and Se pellets (0.118 g) as a chalcogen source were introduced to the other side. The quartz ampoule volume was 25 ml with size of 1,0 cm inner diameter and 32.5 cm in length. The precursors inside the ampoule were degassed at room temperature under dynamic vacuum-pumping process for 1 hour and then the ampoule was sealed at a vacuum level of 1.3×10^{-2} mbar. The sealed ampoule was then placed into a pre-heated two-zone tube furnace, which enables precise control and regulation of the temperature of both zones. In this setup, the vapor pressure of the Se source was determined and controlled by the lowest temperature in the system. The temperature zone (zone 1) in which the Sb source was placed was kept at 500 °C and the Se source (zone 2) varied for the 2 samples, being 380°C for sample 1 (Sb-rich) and 450°C for sample 2 (stoichiometric), which corresponds to the partial pressure of Se of 2.67 mbar and 16.4 mbar, respectively. Since it was not clear, how long synthesis time should be used, 3 hours and 96 hours were used for sample 1 (Sb-rich) and sample

2 (stoichiometric), respectively. Finally, the ampoule was taken out from the furnace and cooled down naturally to room temperature with a cooling rate of 120°C/min.

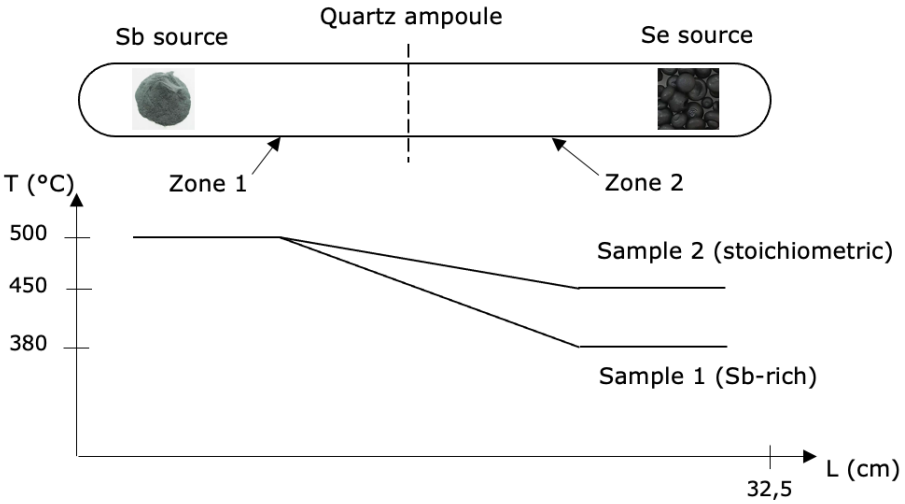

Figure 2.2: Schematic graph of two-temperature zone furnace and the temperature profile for Sb_2Se_3 synthesis.

2.2 Material characterization methods

2.2.1 X-ray diffraction (XRD)

XRD is used for characterizing crystalline materials. The technique provides information on crystal structures, phases, preferred crystal orientations (texture), and other structural parameters, such as lattice parameters, average grain size, crystallinity, strain, and crystal defects. The diffraction pattern is produced by constructive interference of a monochromatic beam of X-rays scattered at specific angles from each set of lattice planes in a sample. The peak intensities are generated by the distribution of atoms within the lattice. Eventually, the X-ray diffraction pattern gives a unique fingerprint of atomic arrangements present in the sample [50].

In the present thesis, XRD was used for the detection of the phase composition of the two microcrystalline powders. The measurement was carried out with Smartlab (Rigaku) Ultima IV diffractometer equipped with rotating 9 kW Copper anode X-ray tube (λ = 0.154 nm, at 40 kV and 40 mA) in Bragg Brentano geometry (10°–70° 2θ angle range with 0.02° step). Reference XRD pattern was simulated from Sb_2Se_3 PDF Card file obtained from crystallographic open database. Lattice constants were identified manually to match experimental XRD peak positions based on orthorhombic crystal system.

2.2.2 Energy-dispersive X-ray spectroscopy (EDX)

EDX is an X-ray-based technique, which is used to describe the chemical composition of materials. While the sample is bombarded with high-energy electrons, the electrons are ejected from the inner shell of the studied atoms producing an electron vacancy. This vacancy is then filled by an electron from a higher energy level. This transfer of electrons releases energy in the form of X-rays and these characteristic X-rays are detected by the EDX. By measuring the characteristic X-ray energy and intensity of each element's X-rays, the elements, as well as their concentration in the sample, are determined [51].

The chemical composition of the two microcrystalline samples were determined by EDX using a Zeiss Merlin high-resolution scanning electron microscope equipped with the Bruker EDX-XFlash6/30 detector (the measurement error is about 0.5 at%).

2.2.3 Raman spectroscopy

Raman scattering is a fast and usually non-destructive technique for investigating the vibrational spectra, phase composition and structural properties of materials. Raman spectroscopy method is based on the inelastic scattering of monochromatic light by the medium, leading to a change in the frequency of the incident light. It provides detailed information about chemical structure, phase and polymorphy, crystallinity, and molecular interactions of materials in any state (solids, liquids, gases). Each material has its unique Raman spectrum as the lattice vibrations depend on the mass of the vibrating atoms as well as on the bond strengths between them [16]. The information depth of this technique depends on the wavelength of the incident monochromatic light as well as on the absorption coefficient of the material under examination. In this thesis, Raman spectroscopy was used for determining the phase composition of the microcrystals. According to the literature, the set of Raman active zone center phonon modes of Sb_2Se_3 have the following symmetries predicted by group theory: $\Gamma = 10A_g + 5B_{1g} + 10B_{2g} + 5B_{3g}$, where A modes are symmetric and B anti-symmetric, respectively [52].

Room temperature Raman spectroscopy was carried out using Micro-Raman spectrometer HORIBA LabRAM 800HR. In this study, a Nd:YAG laser beam with a wavelength of 532 nm is used for the excitation and is focused on the sample by using a x50 objective. This results in a spot size of around 10 micrometers in diameter and a penetration depth of 100 nanometers. The scattered laser light is analyzed by using the 1800 lines/mm grating monochromator and a Si CCD detector. The system enables spectral resolution of 0.5 cm^{-1}. The measurement has been performed using the filter D2 reducing the initial laser power 100 times in order to avoid damage of the sample

surface. The measurement range was from 50 to 550 cm^{-1} as the Raman spectrum of Sb_2Se_3 and possible secondary phases such as Sb_2O_3 lies in this spectral region. The scan time was 100-150 seconds. Lorentzian peaks were used for fitting and analyzing the spectra in each dataset using the Fityk software. Consequently, the resulting peak position values were compared across datasets with the values available in the literature to determine the phase composition of the studied samples. The full width at the half maximum (FWHM) values of the dominating Raman peaks were used for evaluating the crystalline quality of the samples.

2.2.4 Photoluminescence spectroscopy

Temperature dependent PL measurement (the PL setup is shown in Figure 2.3) was carried out using a closed-cycle helium cryostat (Janis CCS-150) to measure the PL spectra at temperatures from 20 K to 180 K. The crystals were glued with a cryogenic grease on a copper plate and mounted on the cold finger of the cryostat. The temperature was controlled via temperature controller (LakeShore Model 321) that enables to measure computer controlled automatic temperature dependence. For PL excitation, a He-Cd laser with the wavelength of 441 nm was used. An optical chopper is used for modulating the incident laser beam on the sample in order to distinguish and amplify the resulting PL signal reaching the detector.

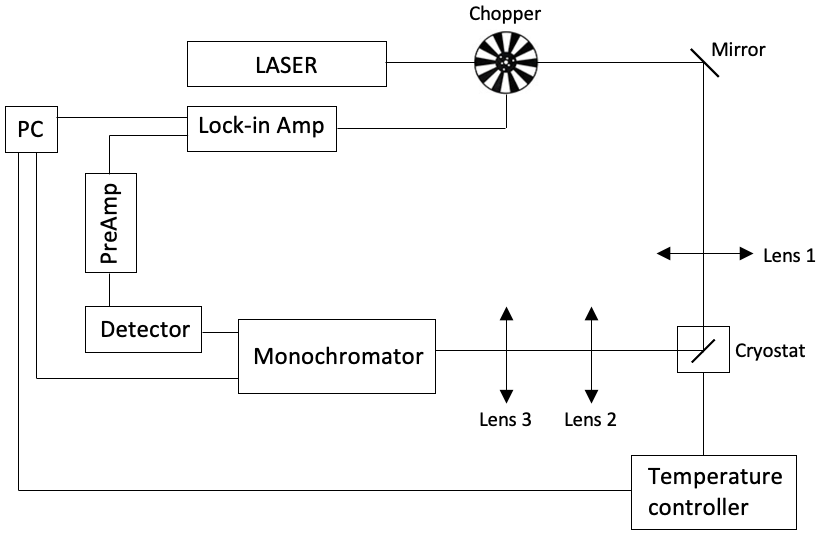

Figure 2.3: Schematic description of the PL setup.

The emitted light was conditioned using a cut-off low-pass filter and focused on the lateral entrance of the computer-controlled single grating (600 mm^{-1}) monochromator

(f = 0.64m) (Horiba Jobin Yvon FHR640). Luminescence was dispersed by the monochromator and detected by the Hamamatsu InGaAs photomultiplier tube. For amplifying the PL signal, a Stanford SR810 DSP lock-in amplifier was used. For the laser power dependent measurements of the PL spectra, neutral density filters were used for altering the power of the incident laser beam. The excitation power was varied in the range from 0.77 to 37.1 mW. The laser power dependent PL measurements were carried out at T = 20 K.

3. RESULTS AND DISCUSSIONS

3.1 Elemental composition

To determine the elemental composition of microcrystals (see SEM image in Figure 2.1) energy dispersive X-ray spectroscopy technique was employed. EDX is showing Sb-rich Sb_2Se_3 (42 at% of Sb and 58 at% of Se) composition for sample 1 and stoichiometric Sb_2Se_3 composition (ratio of Sb:Se atoms 2:3) for sample 2. The samples are accordingly named as Sb-rich Sb_2Se_3 and stoichiometric Sb_2Se_3. In addition, elemental Sb as separate crystals was found in sample 1, which most probably resulted from the un-reacted Sb precursor due to too short synthesis time at chosen synthesis temperature. No secondary phases were found in sample 2.

3.2 Structural and phase analysis

The structural properties of microcrystals were investigated by Raman spectroscopy and X-ray diffraction method. The Raman spectrum of the studied Sb_2Se_3 microcrystals is presented in Figure 3.1 The spectrum was fitted by using Lorentzian curves indicated as dashed lines in Figure 3.1. The characteristic Raman spectrum of Sb_2Se_3 consisted of 6 Raman peaks at 99, 125, 155, 185, 191, and 212 cm^{-1} for Sb-rich and at 99, 125, 155, 186, 192, and 212 cm^{-1} for stoichiometric sample, the Raman peak at 191 and 192 cm^{-1} being the dominant one for each sample, respectively. The both collected Raman spectrums display very similar results and they are in agreement with previously reported literature data by Grossberg et al. [10] and Shongalova et al. [53].

Shongalova et al. [28] reported, that the most intense peak at 190 cm^{-1} is characteristic of Sb-Se stretching mode and it is pointed as an A_g mode. The peak at 155 cm^{-1} can be associated with Sb-Sb bonds, corresponding to the B_{1g} mode. The vibration modes at 125 and 212 cm^{-1} are related to Se-Se bonds, which are assigned to A_g modes. The often-found Raman mode around 250 cm^{-1} and the small shoulder close to the 252 cm^{-1}

[1] peak which are indicating Sb_2O_3 and amorphous Se respectively, could not be detected in our samples. Eventually, no contribution from secondary phases to the Raman spectrum could be monitored [39].

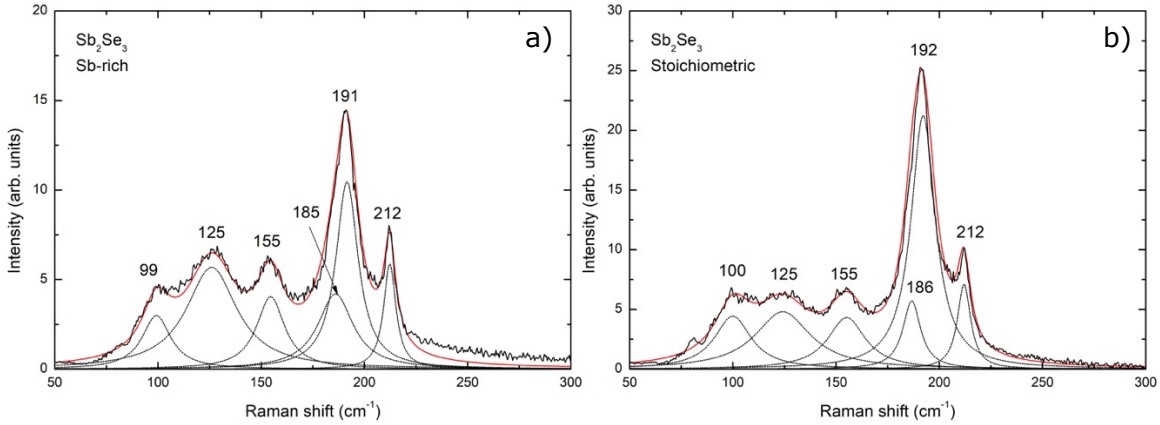

Figure 3.1: The Raman spectrum of the studied a) Sb-rich and b) stoichiometric Sb_2Se_3 microcrystals. The dashed lines indicate to the Lorentzian peaks used for fitting the spectra.

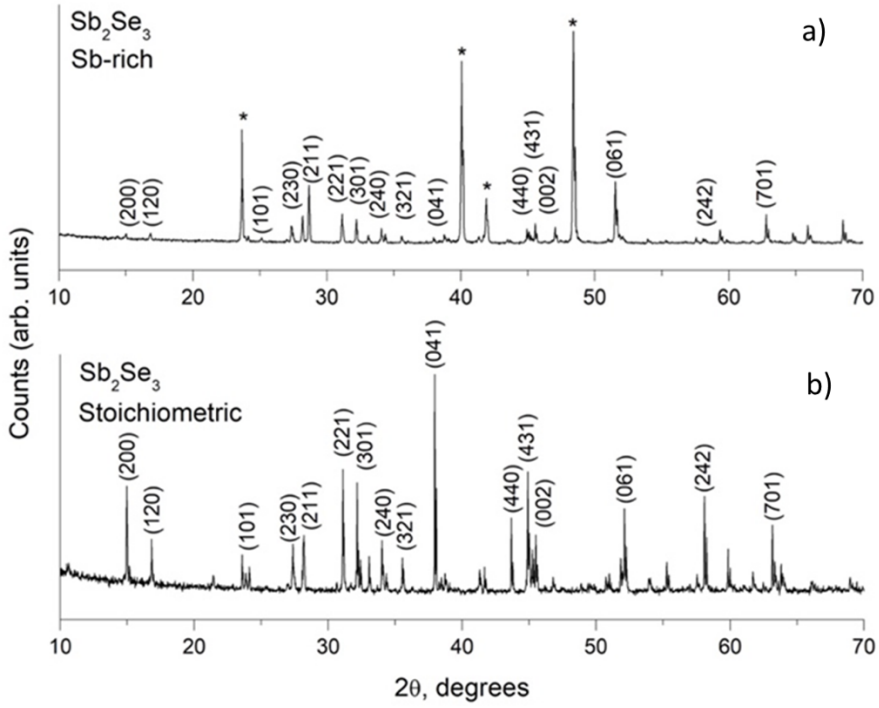

Figure 3.2: The XRD pattern of the studied a) Sb-rich and b) stoichiometric Sb_2Se_3 microcrystals. The asterisk (*) indicates to the dominating XRD peaks of elemental Sb found in Sb-rich Sb_2Se_3.

The XRD pattern of the studied Sb_2Se_3 microcrystals is displayed in Figure 3.2. According to the analysis with respect to PDF_00-015-0861, both materials crystallize in orthorhombic structure of Sb_2Se_3 with space group Pbnm #62. The main diffraction

peaks showing the characteristic structure of Sb_2Se_3 are marked on the XRD pattern of both Sb-rich and stoichiometric Sb_2Se_3 crystals. In the Sb-rich sample, strong contribution of the elemental Sb to the XRD pattern is detected (see Figure 3.2.a) as was also detected by EDX. According to the peak positions, estimated lattice parameters of the Sb-rich sample are a = 1.1670 nm, b = 1.1801 nm and c = 0.3975 nm and for stoichiometric sample a = 1.1650 nm, b = 1.1784 nm, and c =0.3980 nm. These values are in good agreement with the data reported in the literature [10], [38] and in the crystallographic database.

3.3 Photoluminescence of Sb-rich Sb_2Se_3 microcrystals

The photoluminescence spectrum of Sb-rich sample at 20 K is presented in Figure 3.3. The graph presents the fitting of the spectrum with an empirical asymmetric double sigmoid (ADS) function [54] resulting in two PL bands positioned at 1.12 eV (PL1) and 0.85 eV (PL2).

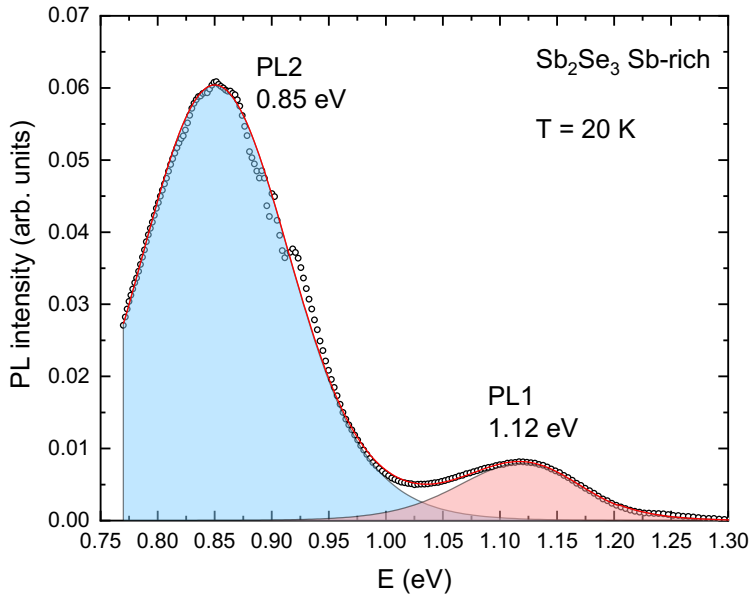

Figure 3.3: Low-temperature PL spectrum of Sb-rich Sb_2Se_3 microcrystals with the result of spectral fitting with ADS function.

The temperature dependence of the PL spectrum between 20 and 180 K is presented in Figure 3.4. The PL band peak positions (Figure 3.5) revealed a shift towards lower energies with the rising temperature in the case of both PL bands. The PL1 peak position follows the temperature dependence of the band gap energy of Sb_2Se_3 [24] indicating to the involvement of the band states in the corresponding recombination mechanism.

PL2 band on the other hand shifts very slowly towards lower energies with increasing temperature indicating to the DAP recombination. Rapid thermal quenching of the PL1 band was observed above T = 60 K, while the PL2 band showed much slower quenching. The thermal quenching of the PL bands is often used to get information about donor and acceptor states behind the defects [41]. Figure 3.6 shows the Arrhenius plot of the thermal quenching of PL1 and PL2 bands, which was fitted by using the theoretical expression for discrete energy levels Eq. (1.1). Obtained thermal activation energies for PL1 and PL2 bands are $E_{T(PL1)}$ = 60±5 meV and $E_{T(PL2)}$ = 143±4 meV, respectively.

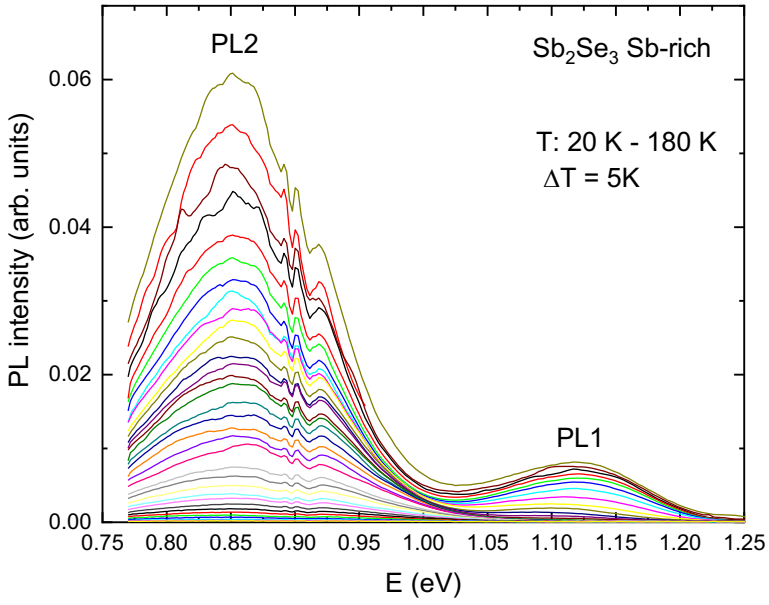

Figure 3.4: The temperature dependence of the PL spectrum of Sb-rich Sb_2Se_3 microcrystals.

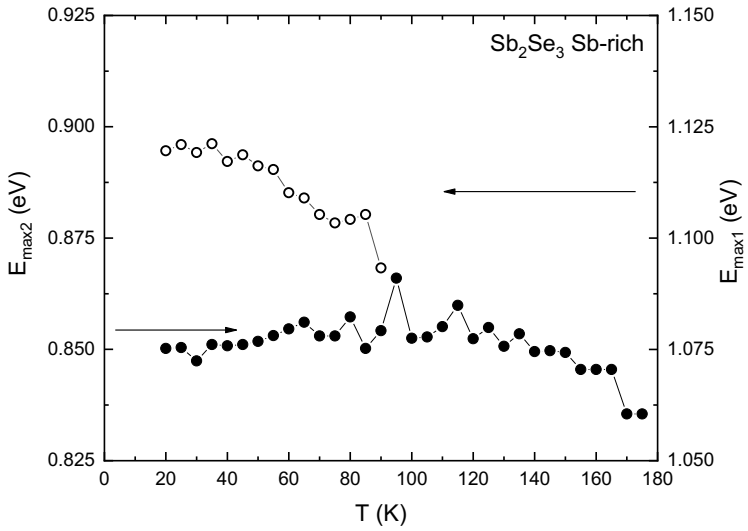

Figure 3.5: The temperature dependence of the PL band peak positions of Sb-rich Sb_2Se_3 microcrystals.

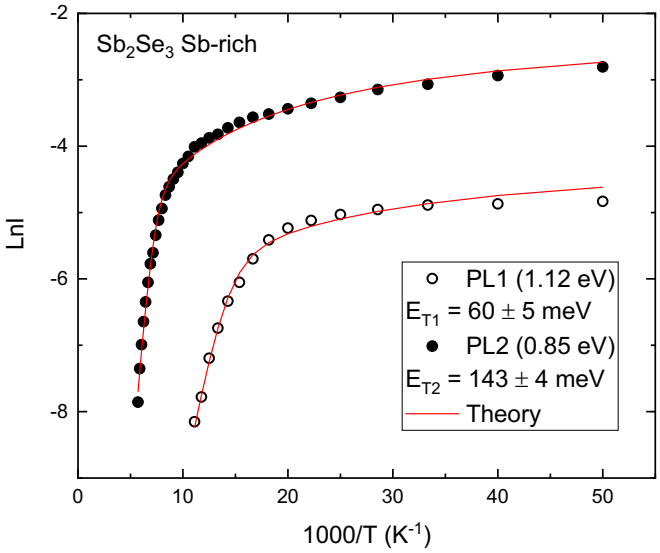

Figure 3.6: The Arrhenius plot showing the thermal activation energies for two PL bands of Sb-rich Sb_2Se_3 microcrystals obtained from the fitting of the curves with Eq. (1.1).

To analyze the recombination mechanisms behind the PL bands, also the laser power dependence of the PL spectra was measured at T = 20 K, see Figure 3.7. The laser power dependencies (from 0.77 to 32.7 mW) of PL band peak positions and intensities are presented in Figures 3.8 and 3.9, respectively. As can be seen in Figure 3.9, the laser power dependence of the PL intensity for both bands follows the relation $\Phi \sim P^k$ and k values of 0.7 and 0.6 were found for PL1 and PL2 indicating to a defect related recombination. The peak position of PL2 band shifts slightly towards higher energies with increasing excitation power, while in case of PL1 band no shift was observed. The rate of the detected blueshift for PL2 band is 1 meV per decade of the laser power, which is characteristic to donor-acceptor pair recombination. At low excitation laser intensities, the recombination is involving DAPs with different distance. On the other hand, at high enough excitation laser intensities the main contribution to the DAP recombination comes from the closer pairs. Distant DAP recombination saturates at high excitation laser powers, whereas close pairs have a larger transition probability and can accommodate more carriers. Therefore, when the excitation power increases, a shift of the PL band peak energy to higher energies is observed [47]. Thus, in our case, the quite small shift of PL2 band peak position with excitation power suggests that the recombination is originated by very close donor-acceptor pairs.

Sb_2Se_3 has a binary chemical composition, yet due to the low symmetry of the atomic sites, the defects are surprisingly complicated and unique. Same type of point defects

located in different atomic sites can lead to different recombination. Furthermore, the uncommon defects that are rarely seen in other semiconductors, have a higher tendency to form in Sb_2Se_3. The reason for this lies behind the weak van der Waals bonds and the large distance between the covalently bonded ribbons [29]. Both, the antimony and selenium atoms are affected from the low-symmetry of the unit cell. Accordingly, there are two different lattice sites for Sb and three different lattice sites for Se [55]. Since the PL2 band involves DAP with very close pairs, (so-called deep donor-deep acceptor pair – DD-DA pair) the donor and acceptor defects engage with the closest Se and Sb sites in the lattice. The closest four Se-Sb pairs and their corresponding Coulomb energies as well as donor ionization energies E_d (see Table 3.1) were calculated using Equation (1.2), considering E_{DA} = 0.85 eV, E_g = 1.333 eV [38], ε = 24 [19] and E_A = 0.143 eV. The resulting E_D values are very close to each other.

Table 3.1: The calculated Coulomb energies and corresponding donor ionization energies for the four most probable close DAPs in Sb_2Se_3. Sb-Se bond lengths are taken from [55].

Bond length (Å)	Coulomb energy (eV)	Donor ionization energy, E_D (eV)
Sb(2)-Se(1): 2.588	0.232	0.572
Sb(1)-Se(3): 2.664	0.225	0.565
Sb(1)-Se(2): 2.678	0.224	0.564
Sb(2)-Se(3): 2.803	0.214	0.554

The calculations using density functional theory by Liu et al. [17] show that the deep level donor defects like V_{Se} and Sb_{Se} are more likely to form in the Sb-rich environment. This partly confirms the fact that the high-efficiency thin-film solar cells having Sb_2Se_3 absorber layer are fabricated under Sb-poor conditions [29]. Moreover, Wen et al. [21] detected a defect with a binding energy of 0.610 eV below the conduction band in DLTS measurements and attributed it to antimony antisite (Sb_{Se}), which shows a very similar E_D value with the donor ionization values calculated for PL2 band [21]. The acceptor defect involved in the DAP recombination behind PL2 band is most probably Se_{Sb} with ionization energy E_A = 0.143 eV as determined from the Arrhenius plot in Figure 3.6. This is in good correlation with Se_{Sb} acceptor ionization energies obtained in other studies that were summarized in Table 1.1. As a conclusion, we can say that the PL2 band in Sb-rich Sb_2Se_3 is originated from DAP recombination most probably involving Sb_{Se} and Se_{Sb} defects.

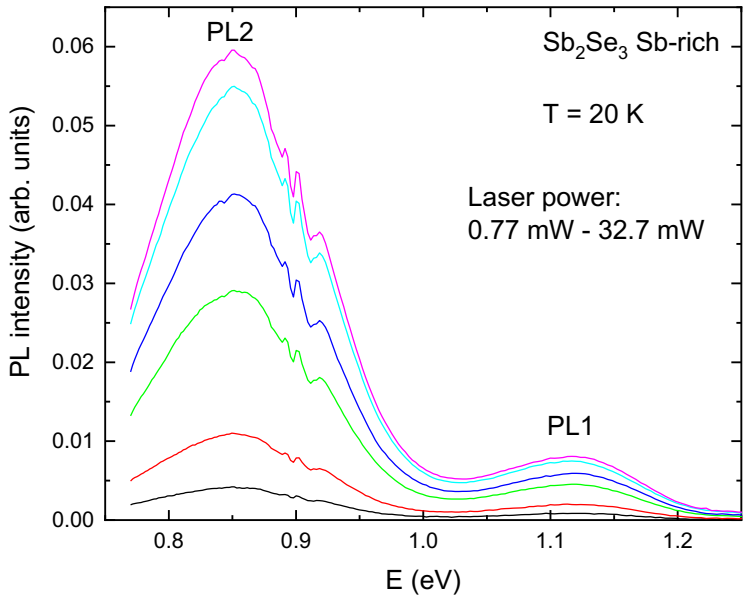

Figure 3.7: Laser power dependence of the low-temperature PL spectrum of Sb-rich Sb_2Se_3 microcrystals.

The PL1 band exhibits a different behavior than the PL2 band and must originate from different type of recombination. The temperature dependence of PL1 band peak position and the temperature dependence of band gap energy are showing comparable behavior, where both spectrums shift to lower energies with similar magnitudes [9]. The observed red-shift of the peak position with temperature and the fact that it is following the temperature dependence of band gap is the sign, that the band states are associated with the recombination process [10]. This is supported also by the fact that PL1 band is not shifting with changing laser power (see Figure 3.8). Nevertheless, considering the PL1 band position at 1.12 eV, the value of the obtained thermal activation energy of 0.06 eV and the band gap energy of Sb_2Se_3 of 1.333 eV, the detected emission cannot result from band-to-band or free-to-bound recombination. Very similar behavior of a PL band at 1.11 eV in Sb_2Se_3 polycrystals was found by Grossberg et al. [10] and the PL band is proposed to originate from the recombination involving grain boundaries, however, it is not confirmed. At this point, we can propose that we see the same PL band that was seen in Ref [10], however, further studies are needed to clarify its origin.

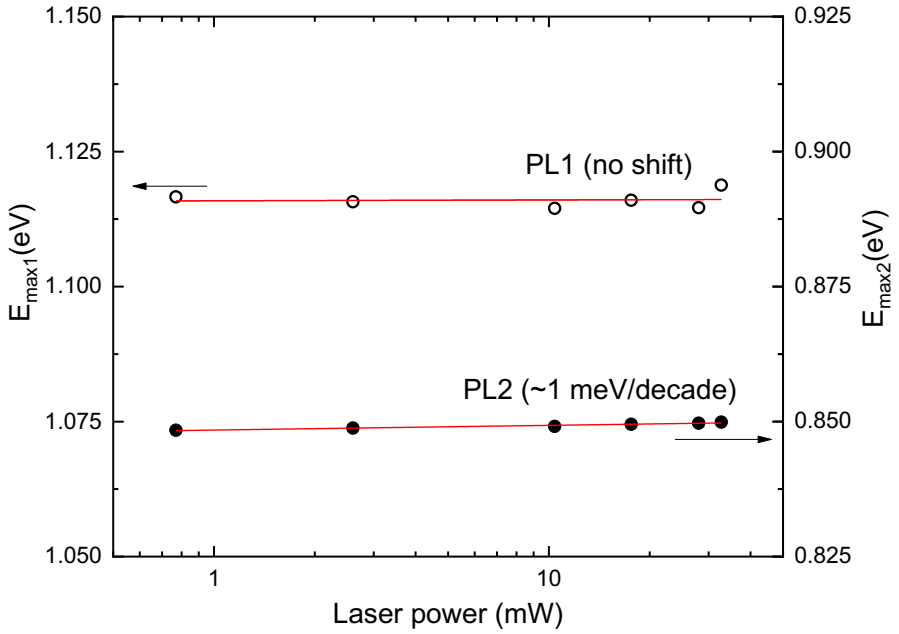

Figure 3.8: The laser power dependence of the PL band peak positions of Sb-rich Sb_2Se_3 microcrystals.

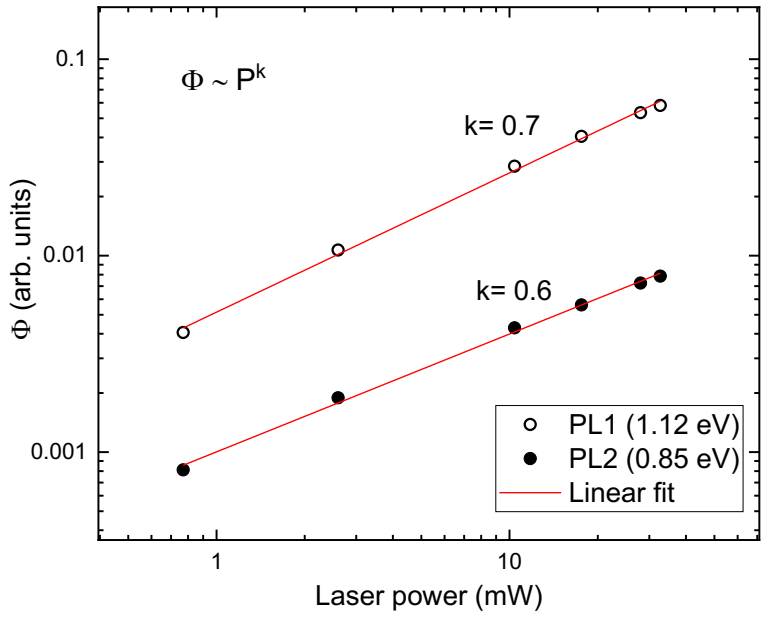

Figure 3.9: The laser power dependence of the PL band intensities of Sb-rich Sb_2Se_3 microcrystals.

3.4 Photoluminescence of stoichiometric Sb_2Se_3 microcrystals

The photoluminescence of the stoichiometric sample at 20 K together with the fitting result using ADS function is presented in Figure 3.10. Three PL bands positioned at 1.26 eV (PL1), 1.04 eV (PL2), and 0.86 eV (PL3) are detected.

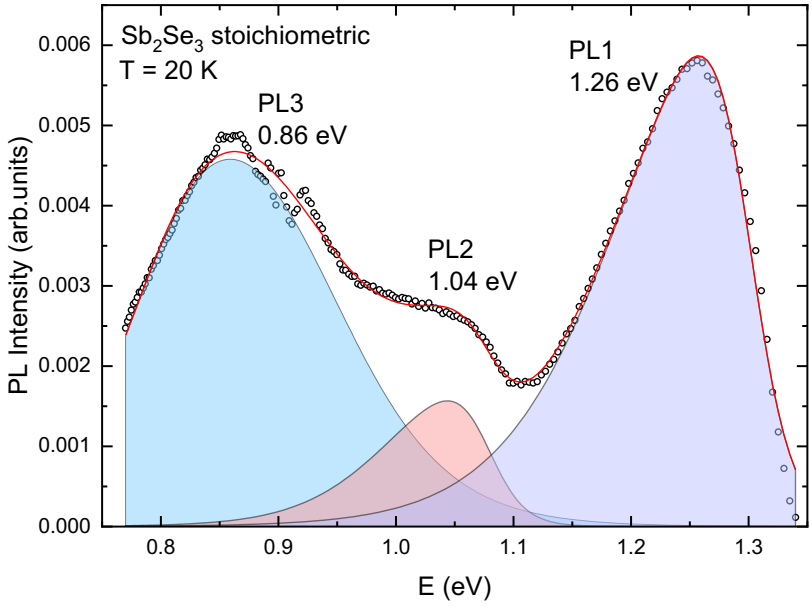

Figure 3.10: Low-temperature PL spectrum of stoichiometric Sb_2Se_3 microcrystals with the result of spectral fitting with ADS function.

The temperature and laser power dependencies of the PL spectrum were measured and are shown in Figures 3.11 and 3.15. The PL2 band quenches very fast with increasing temperature and eventually disappears at T = 65 K. Starting from the same temperature, the PL4 band (1.30 eV) appears at the high energy side of the spectrum, which can be seen clearly from the PL spectra at T = 125 K presented together with the fitting result in Figure 3.12. We observed that the PL1 and PL2 bands have rather an asymmetrical shape and a steeper incline at the high energy side. It is important to mention here that the InGaAs PMT detector rapidly loses its sensitivity starting from 1.3 eV, meaning that the high-energy side of the spectrum is slightly modified by this.

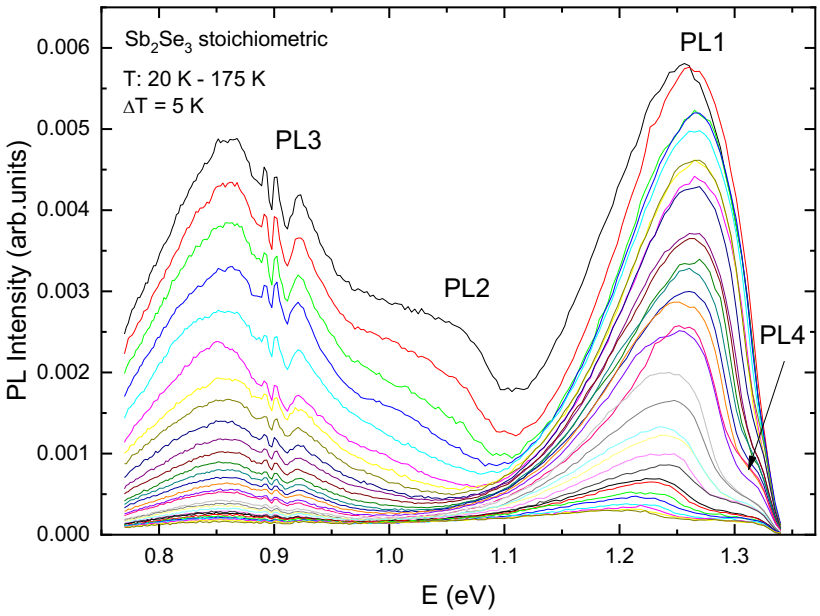

Figure 3.11: The temperature dependence of the PL spectrum of stoichiometric Sb_2Se_3 microcrystals.

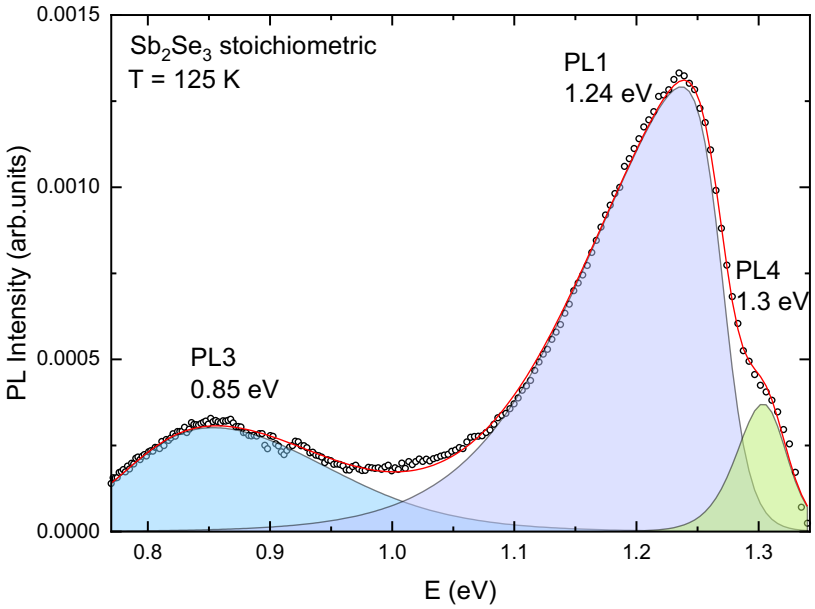

Figure 3.12: PL spectrum of stoichiometric Sb_2Se_3 microcrystals at 125 K with the result of spectral fitting with ADS function.

The temperature dependence of the PL band peak positions (Figure 3.13) reveals an apparent red-shift in the case of PL1 and PL2 bands and a rather small red-shift in the case of PL3 band. The PL1 and PL2 bands follow the temperature dependence of the band gap of Sb_2Se_3 [24]. This behavior is an indication that the band states are involved in the recombination process [10]. In the case of the PL4 band, the peak shifts first to lower energies and then stays constant.

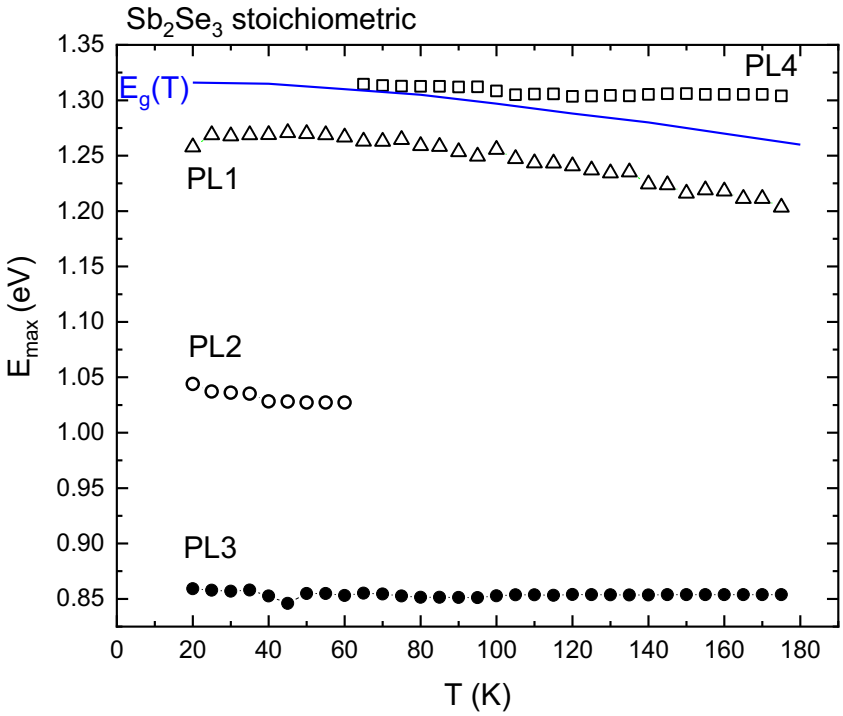

Figure 3.13: The temperature dependence of the PL band peak positions of stoichiometric Sb_2Se_3 microcrystals together with the band gap energy (E_g) from Ref. [24] presented as solid blue line.

As a result of the analysis of the temperature quenching of the PL bands, the Arrhenius plot is displayed in Figure 3.14. The experimental data for the temperature dependence of the integrated PL band intensities were fitted by Eq. (1.1). Calculated thermal activation energies for each peak using the Eq. (1.1) are depicted on the Arrhenius plot. It turned out that all peaks show quite small thermal activation energies 0.06 eV. More precisely 0.052±0.004 eV for PL1, 0.022±0.004 eV for PL2, 0.021±0.005 eV for PL3, and 0.029±0.003 eV for PL4.

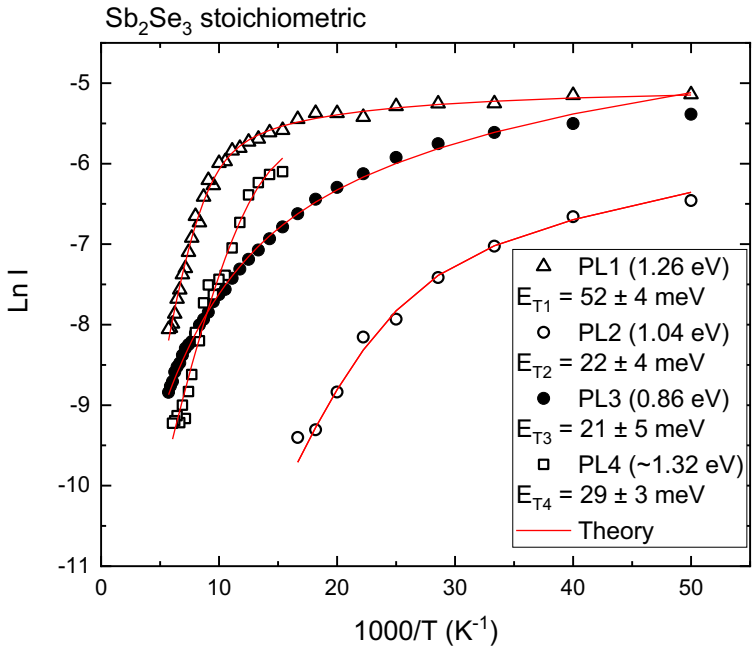

Figure 3.14: The Arrhenius plot showing the thermal activation energies for the PL bands of stoichiometric Sb_2Se_3 microcrystals obtained from the fitting of the curves with Eq. (3.1).

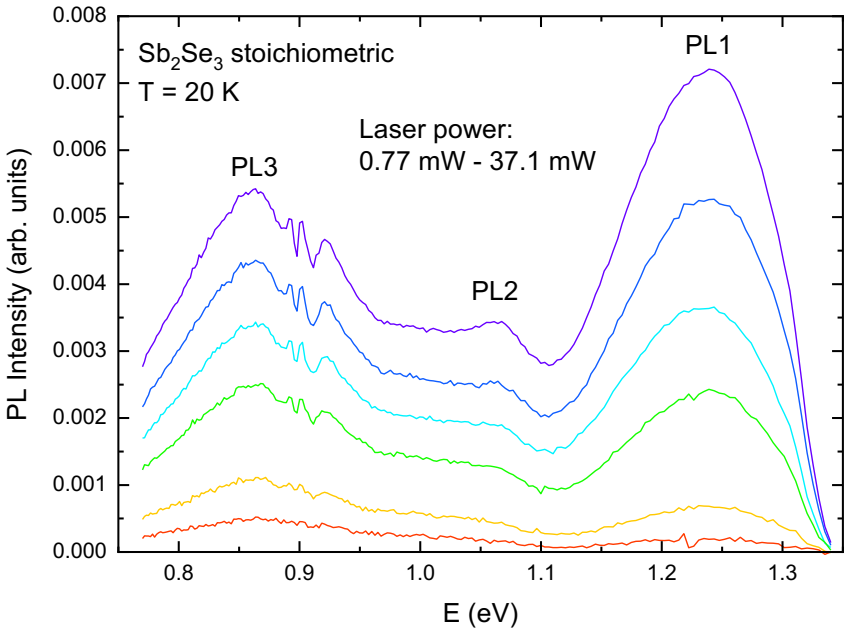

Figure 3.15: Laser power dependence of the low-temperature PL spectrum of stoichiometric Sb_2Se_3 microcrystals.

The laser power dependence of the PL spectrum is presented in Figure 3.15. The spectrum was measured at T = 20 K with different laser excitation powers varied

gradually from 0.77 to 37.1 mW. The peak position of PL2 and PL3 bands blueshifted only slightly with increasing laser power (<1 meV/decade), see Figure 3.16. In the case of PL1, no shift was observed. The laser power dependence of PL band intensities is shown in Figure 3.17. The integrated PL band intensities Φ increase linearly with respect to the laser power P, following $\Phi \sim P^k$. The k values of 0.94, 0.7 and 0.6 were obtained for PL1, PL2 and PL3 bands, respectively, indicating to a radiative recombination of charge carriers localized at defects within the bandgap [10]. Since the PL4 band shows up only after T = 65 K, no analysis about the laser power dependence could be conducted.

Based on the above descriptions of the temperature and laser power dependent behavior of the PL bands in stoichiometric Sb_2Se_3, following conclusions can be drawn. We propose that the PL1 band originates from the free-to-bound recombination involving an acceptor defect with an ionization energy of 0.052±0.004 eV. Considering the PL1 band position at 1.26 eV and the thermal activation energy 0.052 eV, the sum of these two adds up to the band gap of Sb_2Se_3. In addition, the proposed origin of PL1 band (band-to-acceptor recombination) is supported by the fact that this PL band does not shift with laser power and its peak position follows the temperature dependence of the band gap that are characteristic for the free-to-bound PL emission [10]. This is the first time, when this type of PL emission is detected in Sb_2Se_3 and the presence of this type of shallow acceptor defect should be beneficial for the solar cell device performance. Based on theoretical calculations, this shallow acceptor could be V_{Sb} or Se_{Sb} [29].

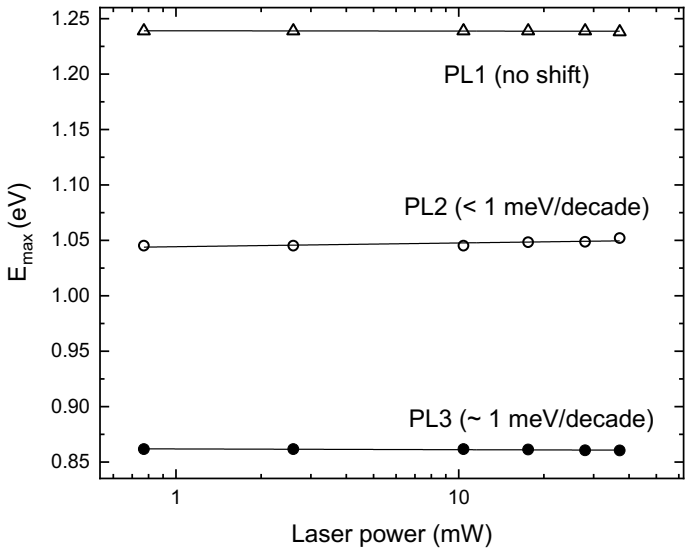

Figure 3.16: The laser power dependence of the PL band peak positions of stoichiometric Sb_2Se_3 microcrystals.

The PL2 band exhibits a similar response with the PL1 band, where the temperature dependence of the peak position shows a red-shift and follows the temperature dependence of the band gap (see Figure 3.13). Besides, the peak position almost doesn't shift with the laser power (see Figure 3.16). These trends prove that the band states are involved in the recombination process. However, considering the PL band peak position at 1.04 eV, the resulted emission could have the same origin as the PL1 band in the Sb-rich sample at 1.12 eV, rather than a band-to-band or free-to-bound recombination. As Grossberg et al. [10] described the PL peak at 1.11 eV, we propose that the PL2 band is originated from the recombination involving grain boundaries, claiming the PL2 band is the same band as the PL1 in the Sb-rich sample and the PL band that was reported in Ref. [10]. However, further studies are needed to clarify its origin.

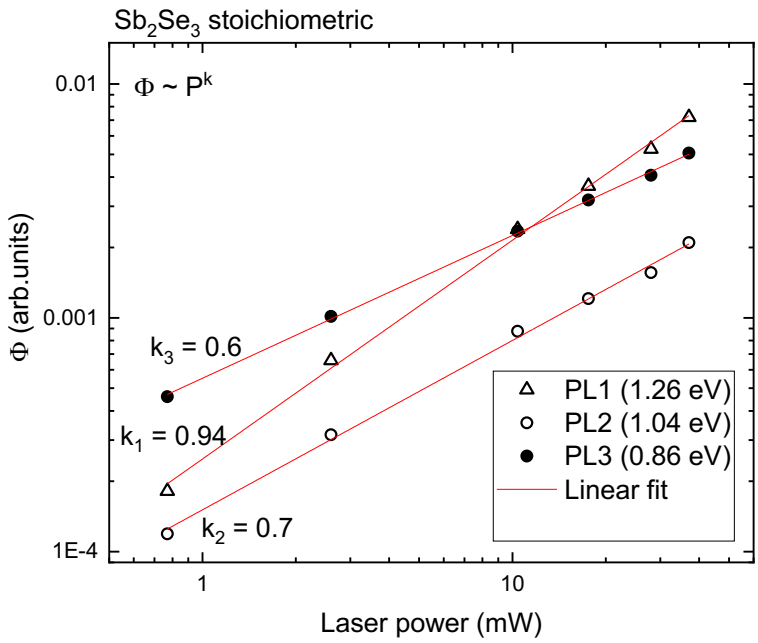

Figure 3.17: The laser power dependence of the PL band intensities of stoichiometric Sb_2Se_3 microcrystals.

The PL3 band regardless of the similar band position at 0.85 eV and 0.86 eV in Sb-rich Sb_2Se_3 and stoichiometric Sb_2Se_3, respectively, seems to have different origin in these two studied samples. Unlike in the Sb-rich Sb_2Se_3, the PL3 band in stoichiometric Sb_2Se_3 shows almost no shift of the PL band position with temperature and the thermal activation energy of the temperature quenching of this deep PL band is only 21 meV. The absence of the temperature dependence of the PL3 band position could indicate that this emission could originate from the intercentral recombination process, which is not

affected by the temperature dependence of the band gap of the material. Also, the small thermal activation energy could be explained by this recombination model. However, as so far there is no evidence of such luminescence centres in Sb_2Se_3, this should be studied further.

Finally, the PL4 band that appears in the spectra from T = 65 K is positioned at 1.3 eV at T = 125 K, which is very close to the band gap of Sb_2Se_3. The interpretation of this PL band is challenging as it is positioned in the spectral region where the detector sensitivity is rapidly decreasing. The PL4 band position follows the temperature dependence of the band gap energy at first and then starting from 100 K stays almost constant. This could be due to the detector sensitivity limit. The near-band-edge emission of the same stoichiometric Sb_2Se_3 microcrystals was recently investigated by Krustok et al. [38], where the PL emission in the spectral region from 1.30 – 1.33 eV is represented by two pairs of free excitons and biexcitons. Unlike in this thesis, where a steady state laser source is used, the measurements in Ref. [38] were done by using very high excitation powers generated by the pulsed laser source. Excitons are often observed in crystals with very high quality and their generation rate is higher at high temperatures and high excitation powers. As a result, in this thesis the PL4 band detected at 1.3 eV at T = 125 K is the same excitonic PL emission observed in Ref. [38] using high excitation powers. The narrow width of the band (0.04 eV) also suggests that PL4 band originates from excitons. Moreover, the PL4 band is showing very similar behavior with the biexciton XX_B at 1.322 eV, which is described in Ref. [38]. Unfortunately, we did conduct laser power dependent PL measurements at higher temperatures due to the low PL signal intensity and cannot therefore compare the corresponding behavior of the PL4 band with the XX_B band in Ref. [38]. Another feature of biexcitons is that they reveal a noticeable red-shift in temperature-dependent measurements, while free excitons usually follow the temperature dependence of the band gap [56]. In our case, the peak position first shifts to lower energies and then stays stable (see Figure 3.13). The reason behind this behavior is probably the fact that the PL4 includes also the contribution of the free exciton X_B at ~1,31 eV in addition to the XX_B peak, but in these measurements these peaks are not resolved as in [38]. However, the PL measurements using steady-state laser enabled us to learn also about the deep defect emission in this stoichiometric Sb_2Se_3 microcrystals.

4. CONCLUSIONS

The purpose of the current study was to investigate the intrinsic defects in Sb_2Se_3 microcrystals with different elemental compositions using PL spectroscopy and to clarify the main radiative recombination processes behind the observed emissions. The PL spectrum of Sb-rich sample revealed two PL bands at 0.85 eV and 1.12 eV, where the deep emission dominates. The PL band at 0.85 eV having high thermal activation energy of 143 ± 4 meV was assigned to a deep donor-deep acceptor pair recombination, considering the detected blueshift with laser power. The calculations showed that the DAP involves a deep donor defect with an ionization energy of 0.572 eV and the deep acceptor defect with ionization energy of 0.143 eV. Based on the findings from the literature and taking the acceptor and donor energy levels into account, the recombination was attributed to Sb_{Se} and Se_{Sb} antisite defects, which are expected to be present in Sb_2Se_3 in high concentrations. The second PL band at 1.12 eV was proposed to originate from a recombination involving grain boundaries based on the same behavior observed for this band previously in the literature However, the origin of this PL band it is not confirmed and needs to be studied further.

During the PL measurements of the stoichiometric Sb_2Se_3 sample, we distinguished four PL bands at 0.86 eV, 1.04 eV, 1.26 eV and 1.3 eV, where the edge emission dominates. The temperature dependence of PL spectrum showed that at higher temperatures starting from 65 K, the band positioned at 1.04 eV disappears and a new peak at 1.30 eV appears. Based on the temperature and laser power dependent behavior of the PL band at 1.26 eV, this band was attributed to free-to-bound recombination involving an acceptor defect with ionization energy of 52 ± 4 meV. This type of PL emission is detected in Sb_2Se_3 for the first time and it should be beneficial for the solar cell device performance as shallow acceptors donate free carriers and increase the p-type conductivity of the material. Based on previously reported defect energy levels the acceptor defect was attributed to V_{Sb} or Se_{Sb}. The second PL band positioned at 1.04 eV, was proposed to have the same origin as the band in the Sb-rich sample at 1.12 eV, which is a recombination involving grain boundaries. Unlike the rest of the PL bands, the third band showed a different kind of behavior, where there was almost no shift of the PL band position with temperature, and the thermal activation energy of the temperature quenching of this deep PL band was only 21 meV. The temperature and laser power dependent behavior of this PL band is rather unusual and it is proposed that this emission may originate from the intercentral recombination process, which is not reported before in Sb_2Se_3 and needs further confirmation. Finally, the PL band at 1.3 eV with narrow width and position very close to the band gap is proposed to originate from the excitonic recombination. Very similar excitonic emission was reported recently for

the same stoichiometric Sb_2Se_3 microcrystals using very high excitation powers generated by the pulsed laser source. However, in this thesis using steady-state laser we were able to learn also about the deep defect emission in the stoichiometric Sb_2Se_3 microcrystals.

Consequently, the results of this PL investigation show that deep defects tend to appear in the Sb-rich sample, whereas in the stoichiometric sample the edge emission dominates. This finding was also supported by theoretical calculations, where detrimental defects are shown to form easily under Se-poor conditions and more benign defects are the dominant defects under Se-rich condition, thus much better photovoltaic efficiency can be achieved under the Se-rich condition. In this study we did not obtain Se-rich samples targeted during the growth, however, our results show that with the decrease in the relative concentration of antimony, the formation of deep defects can be suppressed and shallow defects promoted.
Further studies should be performed to confirm the origin of the PL bands currently attributed to grain boundary related and intercentral recombination.

SUMMARY

This study is focused on the investigation of the defect structure of Sb_2Se_3 using photoluminescence spectroscopy. Photoluminescence is a sensitive method for studying defects and related recombination mechanisms in semiconductors. In the literature, Sb_2Se_3 is presented as a promising photovoltaic absorber material due to its attractive properties and its rapid improvement in the last decade. However, the Sb_2Se_3 based solar cell efficiencies are still far behind the ones of the conventional thin film solar cells and a systematic investigation of the defect structure holds great importance to achieve further progress. In addition to this, the defects in Sb_2Se_3 are surprisingly complicated and unconventional. Moreover, only a few publications about photoluminescence of Sb_2Se_3 are available, which makes the interpretation challenging but also highly essential.

In the scope of the thesis, two different Sb_2Se_3 microcrystals were prepared. Lower temperature and shorter synthesis time resulted in Sb-rich samples while stoichiometric samples were achieved with higher temperature and significantly longer synthesis time. The elemental and phase composition and structural properties were confirmed with EDX, Raman spectroscopy and XRD measurements, respectively. The presence of elemental Sb as a secondary phase was detected in Sb-rich Sb_2Se_3.

The photoluminescence spectra of Sb-rich microcrystals and their dependence on the temperature and excitation power were measured. At T = 20 K, two PL bands positioned at 1.12 eV (PL1) and 0.85 eV (PL2) were observed. The PL1 band is attributed to a recombination involving grain boundaries, yet further studies are needed to clarify its origin. The PL2 band, on the other hand, is proposed to originate from very close donor-acceptor pair recombination probably involving Sb_{Se} and Se_{Sb} defects.

The photoluminescence of the stoichiometric sample at 20 K revealed three PL bands positioned at 1.26 eV (PL1), 1.04 eV (PL2), and 0.86 eV (PL3). Starting from 65 K the PL2 band vanishes and the PL4 band (1.30 eV) appears at the high energy side of the spectrum. The proposed origin of PL1 band is a free-to-bound recombination involving an acceptor defect, which was assigned to V_{Sb} or Se_{Sb}. We suggest that the PL2 band is originated from the recombination involving grain boundaries, claiming the PL2 band is the same band as the PL1 in the Sb-rich sample. Finally, the PL3 and PL4 bands are proposed to originate from the intercentral recombination process and excitonic recombination, respectively.

REFERENCES

[1] IRENA, "Future of Solar Photovoltaic: Deployment, investment, technology, grid integration and socio-economic aspects (A Global Energy Transformation: paper)." International Renewable Energy Agency, Abu Dhabi, 2019.

[2] IEA, "Tracking Report: Solar PV." IEA Publications, Paris, 2020.

[3] J. Ramanujam *et al.*, "Flexible CIGS, CdTe and a-Si:H based thin film solar cells: A review," *Prog. Mater. Sci.*, vol. 110, p. 100619, May 2020, doi: 10.1016/j.pmatsci.2019.100619.

[4] T. D. Lee and A. U. Ebong, "A review of thin film solar cell technologies and challenges," *Renew. Sustain. Energy Rev.*, vol. 70, pp. 1286–1297, Apr. 2017, doi: 10.1016/j.rser.2016.12.028.

[5] "First solar sets new cadmium telluride thin-film cell efficiency record at 22.1%," *Accessed 13 Mar 2021*, [Online]. Available: http://www.pvmagazine.com/news/details/beitrag/first-solar-sets-new-cadmiumtelluride-thin-film-cell-efficiency-record-at-22.1_100023341.

[6] "Solar Frontier Achieves World Record Thin-Film Solar Cell Efficiency of 23.35%," *Accessed 13 Mar 2021*, [Online]. Available: https://www.solar-frontier.com/eng/news/2019/0117_press.html.

[7] Y. Alajlani, A. Alaswad, F. Placido, D. Gibson, and A. Diyaf, "Inorganic Thin Film Materials for Solar Cell Applications," in *Reference Module in Materials Science and Materials Engineering*, Elsevier, 2018, p. B9780128035818103000.

[8] R. Noufi, "High-efficiency CdTe and CIGS thin-film solar cells: Highlights and Challenges," presented at the IEEE 4th World Conference on Photovoltaic Energy Conference, 2006.

[9] C. Chen *et al.*, "Optical properties of amorphous and polycrystalline Sb_2Se_3 thin films prepared by thermal evaporation," *Appl. Phys. Lett.*, vol. 107, no. 4, p. 043905, Jul. 2015, doi: 10.1063/1.4927741.

[10] M. Grossberg, O. Volobujeva, A. Penežko, R. Kaupmees, T. Raadik, and J. Krustok, "Origin of photoluminescence from antimony selenide," *J. Alloys Compd.*, vol. 817, p. 152716, Mar. 2020, doi: 10.1016/j.jallcom.2019.152716.

[11] X. Hu *et al.*, "Investigation of electrically-active defects in Sb_2Se_3 thin-film solar cells with up to 5.91% efficiency via admittance spectroscopy," *Sol. Energy Mater. Sol. Cells*, vol. 186, pp. 324–329, Nov. 2018, doi: 10.1016/j.solmat.2018.07.004.

[12] Z. Li *et al.*, "9.2%-efficient core-shell structured antimony selenide nanorod array solar cells," *Nat. Commun.*, vol. 10, no. 1, p. 125, 2019, doi: 10.1038/s41467-018-07903-6.

[13] F. Kosek, J. Tulka, and L. Štourač, "Optical, photoelectric and electric properties of

single-crystalline Sb_2Se_3," *Czechoslov. J. Phys.*, vol. 28, no. 3, pp. 325–330, Mar. 1978, doi: 10.1007/BF01597220.
[14] R. A. S. P.C.Klippstein, *Growth and characterization of semiconductors*. Bristol, 1990.
[15] T. D. C. Hobson, L. J. Phillips, O. S. Hutter, K. Durose, and J. D. Major, "Defect properties of Sb_2Se_3 thin film solar cells and bulk crystals," *Appl. Phys. Lett.*, vol. 116, no. 26, p. 261101, Jun. 2020, doi: 10.1063/5.0012697.
[16] P. Y. Yu and M. Cardona, *Fundamentals of Semiconductors: Physics and materials properties*, vol. Third, Revised and Enlarged Edition. 2005.
[17] X. Liu *et al.*, "Enhanced Sb_2Se_3 solar cell performance through theory-guided defect control," *Prog. Photovolt. Res. Appl.*, vol. 25, no. 10, pp. 861–870, Oct. 2017, doi: 10.1002/pip.2900.
[18] J. Krustok *et al.*, "Study of point defects in wide-bandgap Cu_2CdGeS_4 microcrystals by temperature and laser power dependent photoluminescence spectroscopy," *J. Phys. Appl. Phys.*, vol. 53, no. 27, p. 275102, Jul. 2020, doi: 10.1088/1361-6463/ab83c1.
[19] C. Chen *et al.*, "Characterization of basic physical properties of Sb_2Se_3 and its relevance for photovoltaics," *Front. Optoelectron.*, vol. 10, no. 1, pp. 18–30, Mar. 2017, doi: 10.1007/s12200-017-0702-z.
[20] H. Deng *et al.*, "High-throughput method to deposit continuous composition spread $Sb_2(Se_xS_{1-x})_3$ thin film for photovoltaic application," *Prog. Photovolt. Res. Appl.*, vol. 26, no. 4, pp. 281–290, Apr. 2018, doi: 10.1002/pip.2980.
[21] X. Wen *et al.*, "Vapor transport deposition of antimony selenide thin film solar cells with 7.6% efficiency," *Nat. Commun.*, vol. 9, no. 1, p. 2179, Dec. 2018, doi: 10.1038/s41467-018-04634-6.
[22] C. N. S. David O. Scanlon, "The Complex Defect Chemistry of Antimony Selenide," *J. Mater. Chem. A*, no. 1–6, 2019, doi: 10.1039/C9TA02022E.
[23] Y. Zhou *et al.*, "Solution-Processed Antimony Selenide Heterojunction Solar Cells," *Adv. Energy Mater.*, vol. 4, no. 8, p. 1301846, Jun. 2014, doi: 10.1002/aenm.201301846.
[24] M. Birkett *et al.*, "Band gap temperature-dependence of close-space sublimation grown Sb_2Se_3 by photo-reflectance," *APL Mater.*, vol. 6, no. 8, p. 084901, Aug. 2018, doi: 10.1063/1.5027157.
[25] K. Zeng D.-J. Xue and J. Tang, "Antimony selenide thin-film solar cells," *Semicond Sci Technol*, vol. 31, no. 6, p. 063001, 2016, doi: 10.1088/0268-1242/31/6/063001.
[26] Pedro Vidal-Fuentes *et al.*, "Multiwavelength excitation Raman scattering study of Sb_2Se_3 compound: fundamental vibrational properties and secondary phases detection," *2D Mater.*, vol. 6, no. 045054, 2019.
[27] A. Mavlonov *et al.*, "A review of Sb_2Se_3 photovoltaic absorber materials and thin-

film solar cells," *Sol. Energy*, vol. 201, pp. 227–246, May 2020, doi: 10.1016/j.solener.2020.03.009.
[28] L. J. Phillips *et al.*, "Current Enhancement via a TiO2 Window Layer for CSS Sb_2Se_3 Solar Cells - Performance Limits and High Voc," *IEEE J. Photovolt.*, vol. 9, no. 2, pp. 544–551, Mar. 2019, doi: 10.1109/JPHOTOV.2018.2885836.
[29] M. Huang, P. Xu, D. Han, J. Tang, and S. Chen, "Complicated and Unconventional Defect Properties of the Quasi-One-Dimensional Photovoltaic Semiconductor Sb_2Se_3," *ACS Appl. Mater. Interfaces*, vol. 11, no. 17, pp. 15564–15572, May 2019, doi: 10.1021/acsami.9b01220.
[30] Y. C. Choi *et al.*, "Sb_2Se_3-Sensitized Inorganic–Organic Heterojunction Solar Cells Fabricated Using a Single-Source Precursor," *Angew. Chem. Int. Ed.*, vol. 53, no. 5, pp. 1329–1333, Jan. 2014, doi: 10.1002/anie.201308331.
[31] Y. Zhou *et al.*, "Thin-film Sb_2Se_3 photovoltaics with oriented one-dimensional ribbons and benign grain boundaries," *Nat. Photonics*, vol. 9, no. 6, pp. 409–415, Jun. 2015, doi: 10.1038/nphoton.2015.78.
[32] L. Wang *et al.*, "Stable 6%-efficient Sb_2Se_3 solar cells with a ZnO buffer layer," *Nat. Energy*, vol. 2, no. 4, p. 17046, Apr. 2017, doi: 10.1038/nenergy.2017.46.
[33] C. Chen *et al.*, "6.5% Certified Sb_2Se_3 Solar Cells Using PbS Colloidal Quantum Dot Film as Hole Transporting Layer," *ACS Energy Lett.*, vol. 2, no. 9, pp. 2125–2132, Sep. 2017, doi: 10.1021/acsenergylett.7b00648.
[34] M. Leng *et al.*, "Selenization of Sb_2Se_3 absorber layer: An efficient step to improve device performance of CdS/Sb_2Se_3 solar cells," *Appl. Phys. Lett.*, vol. 105, no. 8, p. 083905, Aug. 2014, doi: 10.1063/1.4894170.
[35] D.-B. Li *et al.*, "Stable and efficient CdS/Sb_2Se_3 solar cells prepared by scalable close space sublimation," *Nano Energy*, vol. 49, pp. 346–353, Jul. 2018, doi: 10.1016/j.nanoen.2018.04.044.
[36] Y. Lai *et al.*, "Preparation and characterization of Sb_2Se_3 thin films by electrodeposition and annealing treatment," *Appl. Surf. Sci.*, vol. 261, pp. 510–514, Nov. 2012, doi: 10.1016/j.apsusc.2012.08.046.
[37] E. E. Haller and M. D. McCluskey, *Dopants and defects in semiconductors*. Taylor & Francis Group, 2012.
[38] J. Krustok *et al.*, "Identification of Excitons and Biexcitons in Sb_2Se_3 under High Photoluminescence Excitation Density," *Adv. Opt. Mater.*, p. 2100107, Mar. 2021, doi: 10.1002/adom.202100107.
[39] A. Shongalova *et al.*, "Growth of Sb_2Se_3 thin films by selenization of RF sputtered binary precursors," *Sol. Energy Mater. Sol. Cells*, vol. 187, pp. 219–226, Dec. 2018, doi: 10.1016/j.solmat.2018.08.003.
[40] H. B. Bebb and E.W. Williams, *Semiconductors and Semimetals*, vol. Vol 8

Transport and Optical Phenomena. 1972.
[41] A. Jagomägi, "Photoluminescence of Chalcopyrite Tellurides," Ph.D dissertation, Tallinn University of Technology, Tallinn, 2006.
[42] A. Seyhan, "Photoluminescence Spectroscopy of CdS and GaSe," M.S. thesis, The Middle East Technical University, Ankara, 2003.
[43] K. Rudisch, "Defect Engineering in Kesterite Materials for Thin Film Solar Cells," Ph.D dissertation, Uppsala University, Uppsala, 2020.
[44] K. Tanaka, Y. Miyamoto, H. Uchiki, K. Nakazawa, and H. Araki, "Donor-acceptor pair recombination luminescence from Cu_2ZnSnS_4 bulk single crystals," *Phys. Status Solidi A*, vol. 203, no. 11, pp. 2891–2896, Sep. 2006, doi: 10.1002/pssa.200669545.
[45] J. Krustok, H. Collan, and K. Hjelt, "Does the low-temperature Arrhenius plot of the photoluminescence intensity in CdTe point towards an erroneous activation energy?," *J. Appl. Phys.*, vol. 81, no. 3, pp. 1442–1445, Feb. 1997, doi: 10.1063/1.363903.
[46] M. A. Reshchikov, G.-C. Yi, and B. W. Wessels, "Behavior of 2.8- and 3.2-eV photoluminescence bands in Mg-doped GaN at different temperatures and excitation densities," *Phys. Rev. B*, vol. 59, no. 20, pp. 13176–13183, May 1999, doi: 10.1103/PhysRevB.59.13176.
[47] K. Goksen, N. M. Gasanly, A. Seyhan, and R. Turan, "Temperature- and excitation intensity-dependent photoluminescence in Ga_4Se_3S layered crystals," *Mater. Sci. Eng. B*, vol. 127, no. 1, pp. 41–46, Feb. 2006, doi: 10.1016/j.mseb.2005.09.043.
[48] J. Krustok, T. Raadik, M. Grossberg, M. Kauk-Kuusik, V. Trifiletti, and S. Binetti, "Photoluminescence study of deep donor- deep acceptor pairs in Cu_2ZnSnS_4," *Mater. Sci. Semicond. Process.*, vol. 80, pp. 52–55, Jun. 2018, doi: 10.1016/j.mssp.2018.02.025.
[49] J. C. Kim, D. R. Wake, and J. P. Wolfe, "Thermodynamics of biexcitons in a GaAs quantum well," *Phys. Rev. B*, vol. 50, no. 20, pp. 15099–15107, Nov. 1994, doi: 10.1103/PhysRevB.50.15099.
[50] A. A. Bunaciu, E. gabriela Udriştioiu, and H. Y. Aboul-Enein, "X-Ray Diffraction: Instrumentation and Applications," *Crit. Rev. Anal. Chem.*, vol. 45, no. 4, pp. 289–299, Oct. 2015, doi: 10.1080/10408347.2014.949616.
[51] R. K. Mishra and S. Thomas, *Energy-Dispersive X-ray Spectroscopy Techniques for Nanomaterial*. Elsevier Inc., 2017.
[52] N. Fleck, T. D. C. Hobson, C. N. Savory, J. Buckeridge, and T. Veal, "Identifying Raman Modes of Sb_2Se_3 and their Symmetries using Angle-Resolved Polarised Raman Spectra†," *J. Mater. Chem. A*, vol. 1–8, no. 1, 2020, doi: 10.1039/D0TA01783C.
[53] A. Shongalova, M. R. Correia, B. Vermang, J. M. V. Cunha, P. M. P. Salomé, and P. A. Fernandes, "On the identification of Sb_2Se_3 using Raman scattering," *MRS Commun.*,

vol. 8, no. 3, pp. 865–870, Sep. 2018, doi: 10.1557/mrc.2018.94.
[54] J. Krustok, H. Collan, M. Yakushev, and K. Hjelt, "The Role of Spatial Potential Fluctuations in the Shape ofthe PL Bands of Multinary Semiconductor Compounds," *Phys. Scr.*, vol. T79, no. 1, p. 179, 1999, doi: 10.1238/Physica.Topical.079a00179.
[55] V. L. Deringer, R. P. Stoffel, M. Wuttig, and R. Dronskowski, "Vibrational properties and bonding nature of Sb_2Se_3 and their implications for chalcogenide materials," *Chem. Sci.*, vol. 6, no. 9, pp. 5255–5262, 2015, doi: 10.1039/C5SC00825E.
[56] N. Q. Liem, V. X. Quang, D. X. Thanh, J. I. Lee, and D. Kim, "Temperature dependence of biexciton luminescence in cubic ZnS single crystals," *Solid State Commun.*, vol. 117, no. 4, pp. 255–259, Jan. 2001, doi: 10.1016/S0038-1098(00)00454-3.